SACLANTCEN REPORT
serial no: SR- 303

SACLANT UNDERSEA RESEARCH CENTRE REPORT

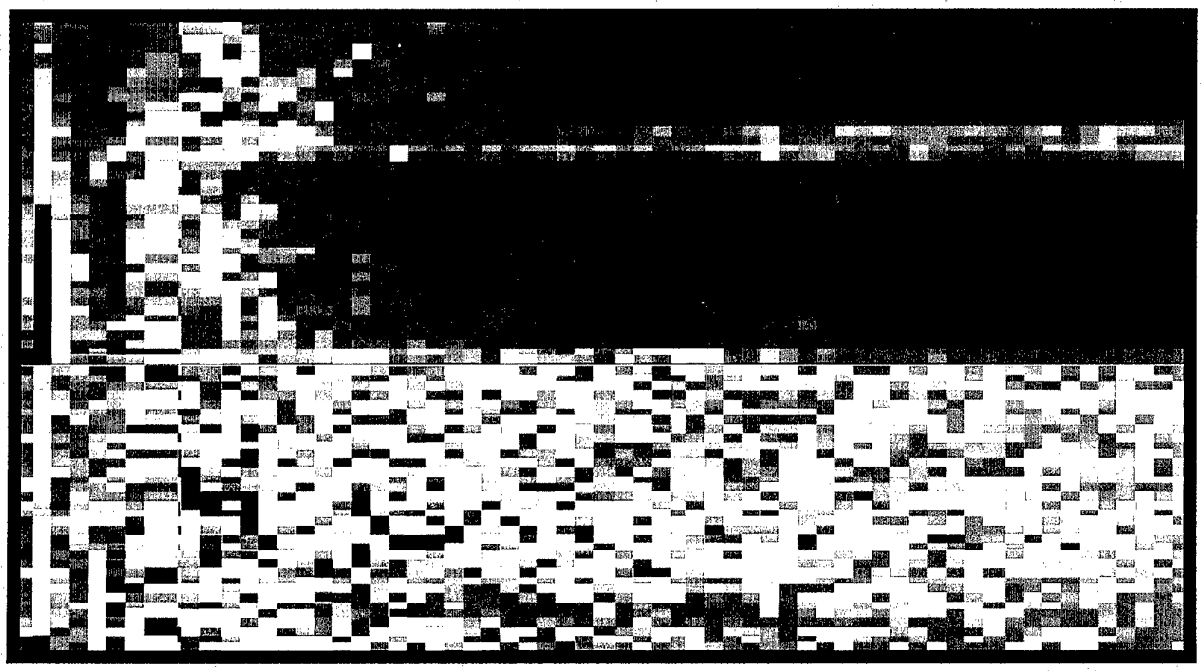

NORTH ATLANTIC TREATY ORGANIZATION ORGANISATION DU TRAITE DE L'ATLANTIQUE NORD

Statistical normalization of non-Rayleigh reverberation

D. A. Abraham

The content of this document pertains to work performed under Project 041-3 of the SACLANTCEN Programme of Work. The document has been approved for release by The Director, SACLANTCEN.

Jan L. Spoelstra
Director

SACLANTCEN SR-303

intentionally blank page

Statistical normalization of non-Rayleigh reverberation

D. A. Abraham

Executive Summary: The primary difficulty in the detection of submarines using low-frequency active sonar in shallow water is reverberation and the numerous false alarms it produces. Automatic detection algorithms are required to analyze this plethora of alarms as well as to reduce operator loading and to improve consistency in performance. Hindering the implementation of automatic detection algorithms is the variability of the statistics of the reverberation from the traditionally assumed Rayleigh distribution, resulting in increased and unknown false alarm performance that changes in range and bearing. This report proffers an algorithm capable of removing the statistical variation of the background reverberation, allowing the implementation of automatic detection algorithms.

intentionally blank page

Statistical normalization of non-Rayleigh reverberation

D. A. Abraham

Abstract: Low-frequency active sonar systems operating in shallow water are primarily limited by reverberation. Reverberation is traditionally assumed to follow a Rayleigh probability distribution, from which the detector and other signal processing algorithms are developed. Experimental studies have shown that reverberation can be non-Rayleigh distributed with varying statistical character over range and bearing. In such a situation, detectors designed under a Rayleigh assumption will exhibit increased and varying false alarm performance. This report develops a technique for dealing with the unknown and varying reverberation statistics by using a non-Rayleigh reverberation model to perform a statistical normalization of the background reverberation. In this manner, range-bearing images will be produced that have a constant background reverberation distribution (i.e., Rayleigh). The technique is evaluated through simulation, with particular attention to the false alarm performance, which is seen to depend on the severity of the non-Rayleighness of the reverberation and the amount of data used to estimate the parameters of the reverberation model. Application to real data has shown that a large degree of the non-stationarity of the range-bearing image can be removed by statistical normalization.

Keywords: non-Rayleigh ○ reverberation ○ constant false alarm rate ○ normalization

Contents

1

Introduction

The detection and localization of submarines using active sonar is often hindered by reverberation from the ocean surface, volume and bottom. In shallow water, reverberation from the bottom typically dominates the other types of reverberation. Normalization algorithms in an active sonar system must remove the non-stationarity of the reverberation prior to performing detection. These algorithms traditionally assume the reverberation to be the result of multiple point scatters, producing a Rayleigh distributed matched filter amplitude with a time-varying scale factor. Thus, the only effect that must be removed is the time-varying scale. Many normalizers have been designed from these assumptions, varying primarily in their methods for dealing with corruption of the auxiliary data used to estimate the mean power level [1, 2, 3, 4, 5]. However, the validity of the multiple point scatterer and resulting Rayleigh assumptions will not hold in all situations. Many researchers (at a variety of grazing angles, beamwidths, frequencies, transmit signal types, and bottom conditions) have shown that bottom reverberation is often non-Rayleigh (see [6] for a comprehensive bibliography). Many of these researchers have attempted to fit observed reverberation to traditional probability distributions, predominantly the log-normal distribution [7, 8, 9, 10] and the Weibull distribution [8, 9]. Others have developed their own models including one based on a Markov driven change between two different types of sea-floor patches [11], a multiplicative model involving chi-squared random variables [12] and a mixture or multi-modal Rayleigh model [13]. It is generally accepted that non-Rayleigh reverberation is caused by small resolution cell sizes resulting in fewer scatterers so that the central limit theorem does not hold [14]. However, it has also been observed that non-Rayleigh reverberation can arise when the composition of the sea-bed varies [11, 15] or when Rayleigh backscatter is affected by a slow modulation as in radar sea-surface clutter [16]. In active sonar, large arrays and wide bandwidth transmit signals can result in small enough range-bearing cells to produce non-Rayleigh reverberation. In low-frequency sonar systems, changes in the bottom composition are almost inevitable over the ranges of interest.

To illustrate the non-Rayleigh character of shallow water reverberation, the probability of false alarm (P_{fa}) measured from some low frequency active sonar data obtained during SACLANT Undersea Research Centre's SCARAB trial in June, 1997 is compared with the Rayleigh distribution in Fig. 1. If, for example, a detection algorithm was designed for a P_{fa} of 10^{-3} assuming Rayleigh reverberation,

the actual P_{fa} in this case would be more than an order of magnitude greater. This illustrates the effect non-Rayleigh reverberation can have on the probability of false alarm in automatic detection algorithms. When the non-Rayleigh character changes with range and bearing, whole regions in a normalized range-beam number display can appear brighter than other more Rayleigh-like regions. The range-bearing display of one ping of SCARAB data shown in Fig. 2 illustrates this where the angular regions to either side of broadside to the array (beam 27) are brighter than other areas. This non-stationarity makes target detection and classification difficult both visually and by automated techniques using multiple beam information such as image processing.

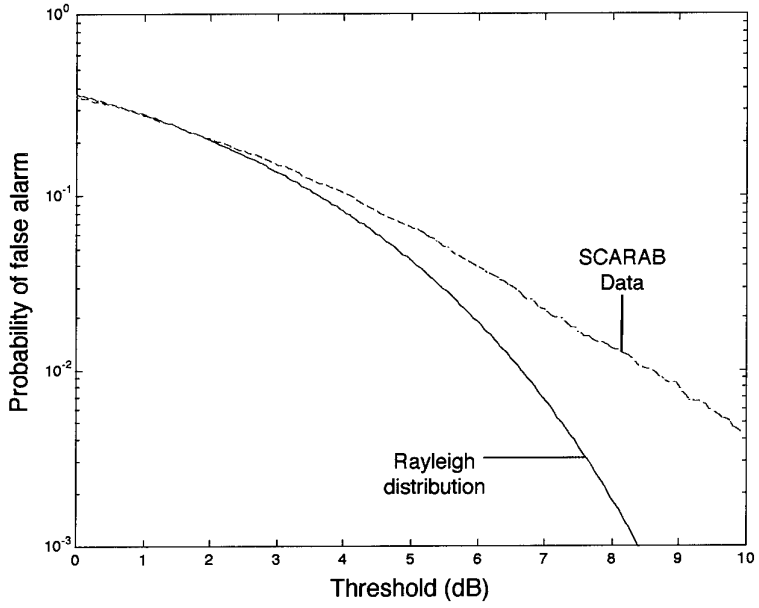

Figure 1 *Probability of false alarm measured from SCARAB data compared with the Rayleigh distribution.*

This report proposes the use of a *statistical* normalizer to convert non-stationary non-Rayleigh reverberation back to the Rayleigh distribution. This is accomplished by approximating the distribution of the reverberation by an appropriate model and applying a nonlinearity to convert the reverberation to the Rayleigh distribution. This concept, along with the Rayleigh mixture reverberation model, is discussed in Section 2. The Rayleigh mixture model is a general model that has been found to adequately represent a wide variety of reverberation [6, 15]. One of the primary difficulties in implementing such a statistical normalizer lies in obtaining target-free auxiliary data. These data are required to estimate parameters describing the distribution of the diffuse reverberation and must not be corrupted by the target

or any target-like coherent reverberation. A nonparametric technique for removing strong interferences from auxiliary data is developed in Section 3. A new method of evaluating the false alarm performance of a normalization algorithm is developed in Section 4 and applied to both the statistical normalizer and the non-parametric interference removal algorithms of Sections 2 and 3. The performance of the combined statistical normalizer/nonparametric interference pruning algorithm is examined through simulation in Section 5 and then applied to low frequency active sonar data obtained from SACLANT Undersea Research Centre's SCARAB97 sea-trial in Section 6.

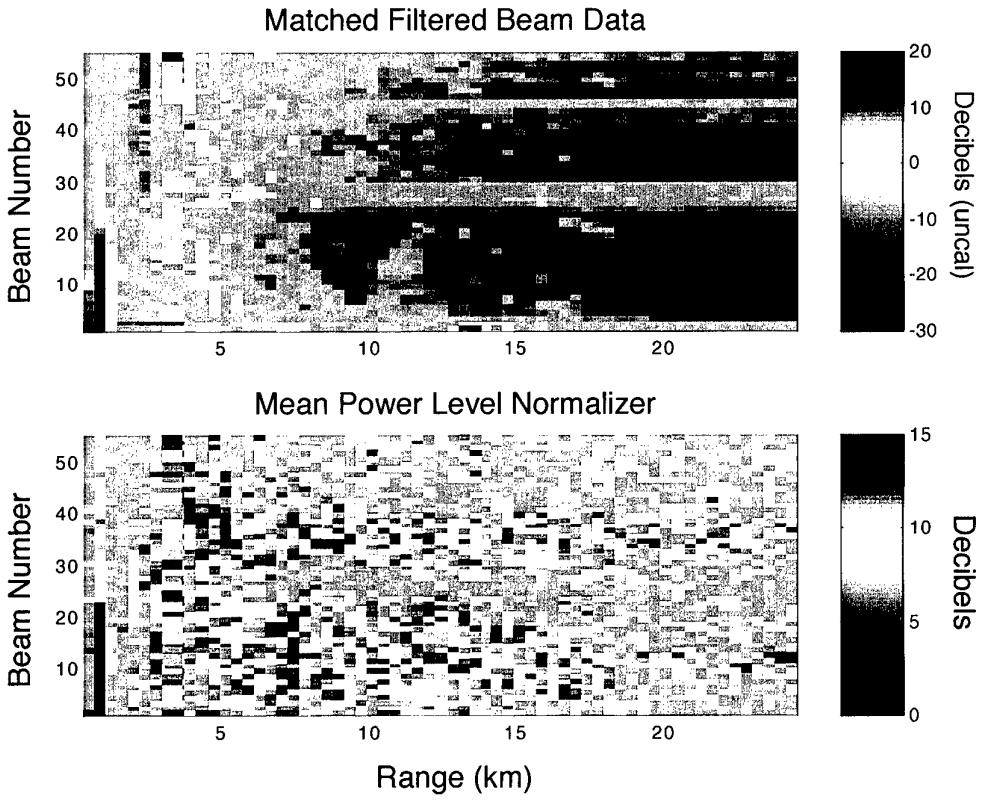

Figure 2 *Range-beam number displays of the matched filtered beam data (upper plot) and the mean level normalizer output (lower plot). The effect of non-Rayleigh reverberation is seen in the normalizer output in angular regions to each side of broadside to the array (beam 27).*

2
Statistical normalization

2.1 Concept

Traditional normalizers assume that reverberation is Rayleigh distributed and are designed to remove the changing mean power level. When no target is present, these mean power level normalizers produce a homogeneous or identically distributed background with a known probability distribution. Detection is then straightforward to perform and allows exact specification of the P_{fa}. When the reverberation is non-Rayleigh, a nonlinearity is required to convert it to being Rayleigh distributed.

Suppose the observed reverberation data X_i have probability distribution function (PDF) $f(x;\Theta)$ and cumulative distribution function (CDF) $F(x;\Theta)$ where Θ is a parameter vector. Consider the random variables obtained by taking the value of the CDF at X_i,

$$U_i = F(X_i;\Theta). \tag{1}$$

The CDF of U_i is

$$\begin{aligned} F_U(u) &= \Pr\{U \le u\} \\ &= \Pr\{F(X_i;\Theta) \le u\} \\ &= \Pr\left\{X_i \le F^{-1}(u;\Theta)\right\} \\ &= F\left(F^{-1}(u;\Theta);\Theta\right) \\ &= u \end{aligned} \tag{2}$$

for $u \in (0,1)$ where $F^{-1}(u;\Theta)$ is the functional inverse of $F(x;\Theta)$, which is assumed to be strictly monotonically increasing over the region $(0,\infty)$ to provide a one-to-one transformation from $X_i \in (0,\infty)$ to $U_i \in (0,1)$. From the CDF $F_U(u) = u$, it is clear that the random variables U_i are uniformly distributed between zero and one; that is, $f_U(u) = 1$ for $u \in (0,1)$. Similarly, it can be shown that the random variables taken by forming

$$Y_i = F_R^{-1}(U_i) \tag{3}$$

will have CDF $F_R(y)$ if the U_i are uniformly distributed between zero and one, $F_R^{-1}(u)$ is the functional inverse of the proper CDF $F_R(y)$, and $F_R(y)$ is strictly monotonically increasing over $(0,\infty)$.

In this manner the observed reverberation may be transformed so that it follows the standard Rayleigh distribution by applying the non-linearity

$$g(x) = F_R^{-1}(F(x;\Theta)) \tag{4}$$

for $x \geq 0$ where

$$F_R(y) = 1 - \mathrm{e}^{-y^2} \quad \text{for} \quad y \geq 0 \tag{5}$$

and

$$F_R^{-1}(u) = \sqrt{-\log(1-u)} \quad \text{for} \quad u \in (0,1) \tag{6}$$

are respectively the Rayleigh CDF and its functional inverse. Now, suppose that the reverberation is Rayleigh with power λ. Then the CDF is simply

$$F(x;\lambda) = 1 - \mathrm{e}^{-\frac{x^2}{\lambda}} \quad \text{for} \quad x \geq 0 \tag{7}$$

and the nonlinearity of eq. (4) becomes

$$g(x) = \frac{x}{\sqrt{\lambda}} \tag{8}$$

which is identical to the traditional mean level normalizers. If the reverberation were Weibull distributed with CDF

$$F(x;\alpha,\beta) = 1 - \mathrm{e}^{-\alpha x^\beta} \quad \text{for} \quad x \geq 0 \tag{9}$$

then the nonlinearity is

$$g(x) = \sqrt{\alpha}\, x^{\frac{\beta}{2}}. \tag{10}$$

To illustrate the transformation required for non-Rayleigh reverberation, the non-linearities required to convert reverberation that is Weibull, K, or Rayleigh mixture distributed are shown in Fig. 3 where the de-emphasizing of the larger values, which pulls in the tails of the reverberation, is clearly seen. The reader is referred to [6] for a complete description of these non-Rayleigh reverberation models. The parameters for the non-Rayleigh distributions were chosen so that the power was one and the kurtosis equal to 1.5 (the kurtosis of a Rayleigh random variable is $\frac{32-3\pi^2}{(4-\pi)^2} - 3 \approx 0.2451$). The Rayleigh mixture had two components with proportions 0.9 and 0.1 and powers chosen according to the specified kurtosis and total power.

From a statistical perspective, the transformation described by eq. (4) is not necessarily the most advantageous one. Ideally, the log-likelihood ratio (LLR) of the data would be used to implement a detector that maximizes the probability of detection while constraining the probability of false alarm. However, if both the LLR and

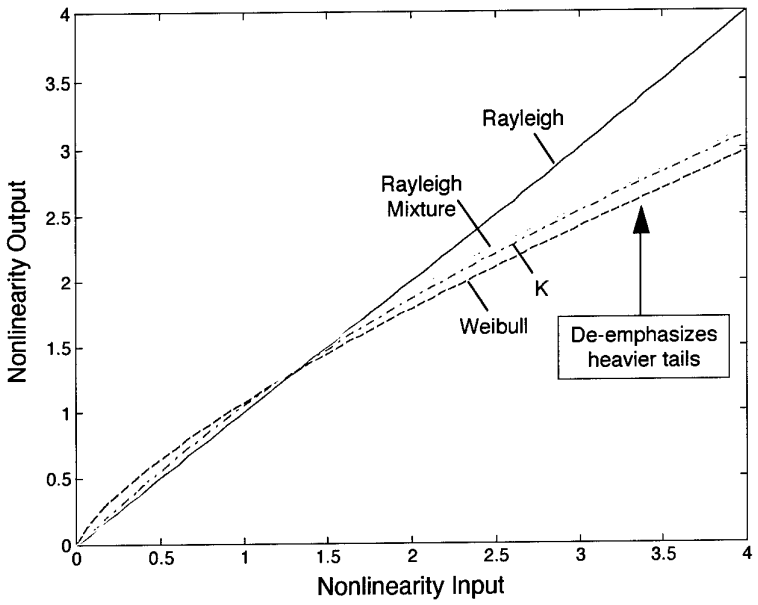

Figure 3 *Example tail de-emphasizing non-linearities for Weibull, K, and Rayleigh mixture distributions with a kurtosis value of* 1.5.

$g(x)$ are monotonically increasing, then either may be used if the detector simply compares each individual matched filter output to a threshold (i.e., no combination of the data over time). Conversely, if the detector combines data from adjacent samples in time, use of the transformed data may not be optimal.

The two primary difficulties in applying the nonlinearity described by eq. (4) are first choosing the appropriate reverberation model $F(x;\Theta)$, and second, estimating the parameters Θ. The Edgeworth expansion, log-normal, Weibull, K and Rayleigh mixture distributions and their parameter estimation are discussed in [6] along with a method for choosing which model best fits the observed data. One of the conclusions of [6] was that the Rayleigh mixture model was the most robust in fitting different types of non-Rayleigh reverberation, a result also supported by [15]. For this reason, the Rayleigh mixture model and its maximum likelihood parameter estimation are described in the following section.

2.2 *Rayleigh mixture model*

The results of [7]–[13] illustrate the variability of the probability distribution of the reverberation amplitude. A single model that is general enough to adequately represent the probability distribution of any encountered reverberation is desired. The lack of sufficient and accurate information about sea-bottom composition, especially over the ranges of interest to low-frequency active sonar, predicates a model independent of environmental parameters. This requirement leads to considering generalized noise distributions such as the generalized Gaussian, generalized Cauchy, stable, or mixture distributions [17]. Many of these generalized noise models describe departures from a nominal distribution which then becomes a special case (i.e., the generalized Gaussian model has as special cases the Laplace and standard Gaussian distributions); however, the mixture model stands out in its flexibility. The mixture model may be used to represent an impulsive component [17], multi-modal data [18], and can accurately represent most distributions given enough components in the mixture.

Under the assumption that the majority of active sonar reverberation will result in a near Rayleigh distribution, a mixture of Rayleigh random variables with different variances may be general enough to adequately describe the reverberation PDF with a minimal parameterization. This is somewhat supported by the results of Stewart *et al.* [13] where good agreement was found between a Rayleigh mixture and the observed reverberation data and by those of Trunk [19] where two component Gaussian mixtures were used to model the quadrature and in-phase parts of the matched filter output for radar clutter. Stronger support may be found in Crowther's [11] model of backscatter from a patchy seabed which simplifies to a two component Rayleigh mixture if the resolution cell size is small compared with the patch size. A further

and more mundane justification for considering a Rayleigh mixture model lies in the ability to obtain the maximum likelihood estimates of the mixture parameters through the expectation-maximization (EM) algorithm [20, 21].

The Rayleigh PDF has form

$$f(x;\lambda) = \frac{2x}{\lambda} \mathrm{e}^{-\frac{x^2}{\lambda}} \tag{11}$$

for $x \geq 0$ where λ is the power (i.e., $\lambda = \mathrm{E}[x^2]$). A mixture of p Rayleigh random variables has the PDF

$$f(x;\Theta) = \sum_{i=1}^{p} \pi_i \, f(x;\lambda_i) \tag{12}$$

for $x \geq 0$ where $\Theta = [\pi_1 \ \cdots \ \pi_p \ \lambda_1 \ \cdots \ \lambda_p]$, π_i is the mixture proportion and λ_i is the power of the i^{th} component. The corresponding CDF is

$$\begin{aligned} F(x;\Theta) &= \sum_{i=1}^{p} \pi_i \int_{s=0}^{x} f(s;\lambda_i) \\ &= \sum_{i=1}^{p} \pi_i \, \mathrm{e}^{-\frac{x^2}{\lambda_i}} \end{aligned} \tag{13}$$

for $x \geq 0$.

Substitution of eq. (13) into the nonlinearity of eq. (4) results in

$$g(x) = \left[-\log \left\{ \sum_{i=1}^{p} \pi_i \, \mathrm{e}^{-\frac{x^2}{\lambda_i}} \right\} \right]^{\frac{1}{2}}. \tag{14}$$

It should also be noted that the standard Rayleigh distribution results if there is only one component in the Rayleigh mixture or if all components have the same power.

Care should be taken in the numerical evaluation of eq. (14), particularly for large values of x where finite precision arithmetic may return a value of zero for the summation even though the summand is always positive (for $\pi_i \neq 0$). A solution is to factor out the largest term in the summation, say $\pi_0 \exp\left\{-\frac{x^2}{\lambda_0}\right\}$, which simplifies further once the logarithm is applied. The resulting summation is then one plus $p-1$ terms between zero and one and may be evaluated without fear of significant numerical error.

2.2.1 Target models

Another distinct advantage of the Rayleigh mixture model is it's ability to incorporate the standard fluctuating and non-fluctuating target models. The Rayleigh

mixture model may be developed from a mixture of zero-mean complex Gaussian random variables for the quadrature and in-phase components of the matched filter output. This differs slightly from the work of Trunk [19] in that this model forces both the quadrature and in-phase components to come from the same mixture component and results in a Rayleigh mixture for the magnitude.

The non-fluctuating target model is represented by a non-zero mean component in the complex matched filter output—essentially adding a constant to the aforementioned mixture of zero-mean complex Gaussian random variables. The resulting magnitude distribution is a mixture of Rician random variables

$$f_{\mathrm{nf}}(x;\Theta,\mu) = \sum_{i=1}^{p} \pi_i \, f_1\left(x;\lambda_i,\frac{|\mu|^2}{\lambda_i}\right) \tag{15}$$

where $\frac{|\mu|^2}{\lambda_i}$ is a signal-to-reverberation power ratio (SRR),

$$f_1(x;\lambda,\delta) = \frac{2x}{\lambda}\mathrm{e}^{-\delta-\frac{x^2}{\lambda}} \, I_0\left(2x\sqrt{\frac{\delta}{\lambda}}\right) \tag{16}$$

is the Rician PDF with scale λ and SRR parameter δ, and $I_0(x)$ is the zero-order modified Bessel function.

The fluctuating target model is represented by an additive zero-mean Gaussian component to the complex matched filter output. This results in a mixture of Rayleigh random variables with power $\tilde{\lambda}_i = \lambda_i + \lambda_0$ where λ_0 is the variance of the target component,

$$f_{\mathrm{fl}}(x;\Theta,\lambda_0) = \sum_{i=1}^{p} \pi_i \, f(x;\lambda_i+\lambda_0) \, . \tag{17}$$

The proof of these results is sketched in Annex A.

2.2.2 *Estimation of the Rayleigh-mixture parameters*

The Rayleigh PDF falls under the exponential family of distributions [22]. Thus, the EM-algorithm may be applied directly from the results of [20] or [21] to obtain the maximum likelihood estimates of the mixture parameters. For the interested reader, this development is provided here in Annex B.

The EM-algorithm for obtaining maximum likelihood estimates of the mixture parameters from the observed data $(x_1, \ldots, x_n)$ is summarized as follows:

1. **Initialize Θ -** For example, set $\hat{\pi}_i = \frac{1}{p}$ and form the $\hat{\lambda}_i$ as the sample power of subsets of the observed data.

2. **Expectation step -** Form the intermediate variables

$$A_{i,j} = \frac{\hat{\pi}_i}{\hat{\lambda}_i} \mathrm{e}^{-\frac{x_j^2}{\hat{\lambda}_i}} \tag{18}$$

and

$$W'_{i,j} = \frac{A_{i,j}}{\sum_{i=1}^{p} A_{i,j}} \tag{19}$$

for $i = 1, \ldots, p$ and $j = 1, \ldots, n$.

3. **Maximization step -** Form new estimates of Θ

$$\hat{\pi}_i = \frac{1}{n} \sum_{j=1}^{n} W'_{i,j} \tag{20}$$

and

$$\hat{\lambda}_i = \frac{\sum_{j=1}^{n} x_j^2 W'_{i,j}}{\sum_{j=1}^{n} W'_{i,j}}. \tag{21}$$

4. **Convergence -** If the normalized change between consecutive estimates of the unknown parameters is greater than some tolerable value, then go to step 2.

As the EM algorithm converges to local and not global maxima, it may be appropriate to run the iteration from several initial starting points. A reasonable initialization for the mixture proportions is to set them to be equally likely, $\hat{\pi}_i = \frac{1}{p}$. Reasonable initial choices for the power components are either (i) the sample powers formed from p disjoint subsets of the n data samples, or (ii) the sample powers formed from p subsets of the n ordered data samples so that $\hat{\lambda}_i < \hat{\lambda}_{i+1}$.

Choice of the model order poses a slightly more difficult problem. It is possible to apply Akaike's information criterion [23] or Rissanen's minimum descriptive length criterion [24] to choose the model order. Other equally justifiable methods include evaluation of the Kolmogorov-Smirnov statistic or consideration of the mixture component proportions and powers (i.e., if an additional component results in a near zero proportion or a power identical to a component already present, the lower order model is likely adequate). Experience has shown that three or fewer components are usually sufficient to represent low-frequency active sonar reverberation.

In applying this method to real data, the time required for convergence becomes an issue owing to the massive number of times the parameter estimation must be performed (essentially once for every range-bearing cell). As it is expected that the non-Rayleigh character of the data will not change too rapidly in range or bearing, the parameter estimation may not need to be performed for every range sample and the time to convergence may be reduce by initializing the algorithm with the most recent set of parameter estimates.

3

Removal of interference from auxiliary data

In constant false alarm rate (CFAR) detection, masking of a target occurs when the estimate of the reverberation power formed from the auxiliary data is unnaturally high, resulting in a reduced probability of detection. This occurs particularly when a target or target-like interference is present in the auxiliary data and results in shadow regions around the interference. Normalizers based on order statistics (OS) [2] are traditionally used to alleviate problems such as masking or its counterpart, false alarm rate inflation. These normalizers use a subset of the ordered auxiliary data to form an estimate of the reverberation power, essentially discarding some of the largest and smallest values. However, they do not utilize any information about the location of the largest or smallest values within the auxiliary data window. Lops and Willett [4] have proposed a CFAR detector that does exploit position information using the L*l*-filters of Palmieri and Boncelet [25]. Their L*l*-CFAR detector is a mean power level normalizer with robust performance when the auxiliary data are corrupted by interference (target-like data) and clutter (regions with higher intensity). However, as previously noted, when dealing with non-Rayleigh reverberation, normalization requires more than simple estimation of the mean in the presence of interferences in the auxiliary data. An uncorrupted sample of the reverberation is required to determine the departure of the distribution from Rayleigh.

If strong range-spread target-like interferences are present in the auxiliary data, removal of some of the largest values would successfully produce a homogeneous (i.e., uncorrupted) sample of reverberation-only data. However, when the auxiliary data are homogeneous, such a process would remove the largest reverberation values. Removal of these extreme values eliminates evidence of heavy tails from the auxiliary data and would result in a flawed estimation of the PDF of the auxiliary data. Thus, an alternative method is required to remove range-spread target-like interferences when they are present and leave the auxiliary data unmodified otherwise. It is possible to prune these interferences from the auxiliary data by exploiting their spatial compactness (in range). This is also the premise of the L*l*-CFAR detector of Lops and Willett [4] where an L*l*-filter is used to estimate the mean power level. Here, however, a decision is made first about the presence of an interference in the auxiliary data followed by removal of the affected data only if it is decided that an interference is present. The resulting pruned auxiliary data is then used to estimate the pertinent reverberation model parameters.

As the PDF of the reverberation will not be known exactly and is expected to change with range and bearing, a nonparametric technique is required to choose between the interference-present hypothesis (H_1) and the null hypothesis (H_0) of independent and identically distributed reverberation data. Let the set $\{K_1, K_2, \ldots, K_n\}$ represent the integer-valued indices to the ordered complete auxiliary data. If $\{X_1, X_2, \ldots, X_n\}$ are the n samples of auxiliary data, then the ordered samples are

$$X_{(1)} \leq X_{(2)} \leq \cdots \leq X_{(n)} \tag{22}$$

and if $X_i = X_{(n-j+1)}$ then $K_j = i$. For simplicity, the indices have been numbered contrary to standard notation for ordered statistics so that K_1 represents the position or index of the largest data sample, K_2 the second largest, down to K_n representing the position of the smallest sample. If the auxiliary data are statistically independent and identically distributed, then the probability of the largest value occurring in the first position, or second, or n^{th} are all equally $\frac{1}{n}$; that is, the probability mass function (PMF) of K_1 is

$$p(k_1) = \frac{1}{n} \quad \text{for } k_1 = 1, \ldots, n. \tag{23}$$

Similar arguments lead to the marginal PMF of any one index

$$p(k_j) = \frac{1}{n} \quad \text{for } k_j = 1, \ldots, n \tag{24}$$

and the joint PMF of any pair of indices

$$p(k_i, k_j) = \frac{1}{n(n-1)} \tag{25}$$

for $k_i = 1, \ldots, n$ and $k_j = 1, \ldots, n$ excepting cases where $k_i = k_j$. Extension to the joint PMF of all the indices results in

$$p(k_1, \ldots, k_n) = \frac{1}{n!} \tag{26}$$

where each index varies between 1 and n and no two indices can have the same value. This result implies that any test statistic formed from the indices to the ordered statistics will be nonparametric under the null hypothesis.

Formulation of an optimal test is not possible due to the vague description of the interference-present hypothesis (H_1) and the difficulty in analyzing the resulting probability mass function (PMF) of the indices to the ordered statistics. However, if an interference is spatially compact and stronger than the underlying noise distribution, it is likely that the indices of the largest order statistics will indicate the position of such an interference within the auxiliary data. This information, accompanied by the fact that all the permutations of the indices to the order statistics are

equally likely under the null hypothesis, leads to considering the distance between the indices pointing to the largest values of the auxiliary data. Suppose only the indices to the two largest samples are considered. The test statistic

$$T_2 = (K_2 - K_1)^2 \tag{27}$$

may provide adequate distinction between H_0 and H_1 if both of the two largest samples are due to the interference. With heavy tailed reverberation, target-like bottom features of unknown size, and spreading of the target return due to the multipath of shallow water and reflection off of a large target, this may not always be the case. Thus, it is prudent to also consider the index to the third largest sample and form a similar test statistic,

$$\begin{aligned} T_3 &= (K_2 - K_1)^2 + (K_3 - K_2)^2 + (K_3 - K_1)^2 \\ &= T_2 + (K_3 - K_2)^2 + (K_3 - K_1)^2 , \end{aligned} \tag{28}$$

which will perhaps perform well if at least two of the three largest samples are due to the interference. Extending this type of test statistic to one considering the m largest samples results in

$$\begin{aligned} T_m &= \sum_{i=2}^{m} \sum_{j=1}^{i-1} (K_i - K_j)^2 \\ &= T_{m-1} + \sum_{i=1}^{m-1} (K_m - K_i)^2 . \end{aligned} \tag{29}$$

If a strong and spatially compact interference exists in the auxiliary data, the pruning statistics T_m should be smaller than when the auxiliary data are uncorrupted. Thus, interference presence may be tested by choosing

$$\begin{aligned} H_0 : &\quad \text{Interference absent if } T_m \geq h_m, \text{ or} \\ H_1 : &\quad \text{Interference present if } T_m < h_m \end{aligned}$$

where h_m is a threshold that is ideally chosen according to a desired probability of falsely declaring an interference present in the auxiliary data (i.e., Type I error). As the spatial extent of the interference is not known a priori, it may be difficult to choose an appropriate value for m. As an alternative, each value of T_m may be considered up to some maximum number $m_{\max}$ which should be much smaller than n (T_n is a constant) and greater than the maximum spatial extent of an interference. Unfortunately, this greatly complicates analysis of the Type I error probability and thus the thresholds h_m. In fact, computation of the PMF of T_m under H_0 is reasonably feasible analytically only for $m = 2$ and numerically so only for small m and n. Thus, it is not possible to exactly determine thresholds h_m based on the probability that $T_m < h_m$ under H_0 for anything but small m.

As the consequence of falsely declaring an interference present in the auxiliary data is the removal of the noise outliers, exact knowledge of the Type I error probability

is not crucial. Thus, approximate thresholds may be obtained by assuming a Gaussian form for the PMF of T_m. The Gaussian PDF is completely determined by its mean and variance, which in this case entails a fairly involved derivation as seen in Annex C. The results are as follows,

$$\begin{aligned} \mathrm{E}[T_m] &= \left[\frac{m(m-1)}{2}\right]\left[\frac{n(n+1)}{6}\right] \\ &= l\left[\frac{n(n+1)}{6}\right] \end{aligned} \tag{30}$$

and

$$\begin{aligned} \mathrm{Var}[T_m] &= l(2c_1 - 8c_2 + 6c_3) + l_0(4c_3 + 4c_4 - 8c_5) \\ &\quad + [l(l-1) - l_0](c_1 - 4c_2 + 3c_3) - l^2\left[\frac{n^2(n+1)^2}{36}\right] \end{aligned} \tag{31}$$

where

$$l = \frac{m(m-1)}{2}, \tag{32}$$

$$l_0 = \begin{cases} 6\binom{m}{4} & m \geq 4 \\ 0 & m < 4 \end{cases} \tag{33}$$

and c_1–c_5 are as described in Annex C. The threshold h_m is then chosen according to a desired probability of Type I error, α, under a Gaussian assumption for T_m,

$$h_m = \mathrm{E}[T_m] - z_\alpha\sqrt{\mathrm{Var}[T_m]}, \tag{34}$$

where z_α is the α-quantile of a Gaussian random variable (Z) with zero mean and unit variance,

$$\alpha = \Pr\{Z > z_\alpha\} = \Pr\{Z < -z_\alpha\}. \tag{35}$$

3.1 Choosing which cells to remove

Once the decision has been made that a spatially compact interference is corrupting the auxiliary data, the affected cells must be removed. Without exact knowledge about the range extent of the interference it is difficult to know how many and which cells to remove. The following nonparametric technique exploits the expected spatial compactness of the interference, additionally allowing the removal of a variable number of cells.

1. Isolate the indices pointing to the m largest values in the auxiliary data sample. Choose m according to the maximum number of possible interference samples (perhaps $m_{\max}$).

2. Form a histogram using equally spaced bins between the smallest and largest indices of the interference subset. The number of bins should be less than or equal to m.

3. Discard any cells within a reasonable distance (say half to two-thirds of the maximum number of interference cells) of the cell yielding the largest frequency from the histogram.

3.2 Discussion

The non-parametric interference pruning (NPIP) algorithm described in the previous sections was developed to deal with the existence of a strong spatially compact interference with unknown range extent that corrupts possibly non-Rayleigh auxiliary data. The objective is to produce an interference-free sample of the reverberation data from which reverberation model parameters may be estimated. The requirement for the procedure to deal with non-Rayleigh reverberation with unknown distribution predicates a non-parametric technique. The strong interference assumption is arrived at by postulating that weak interferences will not greatly alter the reverberation parameter estimation and additionally helps to justify the non-parametric form of the algorithm. The unknown range extent of the interference is required to account for interferences (i.e., bottom features producing coherent rather than diffuse reverberation) of unknown dimension and also for the spreading that an active sonar echo incurs from propagation to and from the target and reflection off of the target. This particular assumption is certainly valid for current tactical sonar bandwidths and array sizes; however, it may need to be reconsidered if no spreading is expected (i.e., if the target and interference are smaller than the resolution cell size).

The NPIP algorithm suffers from one glaring weakness—the lack of consideration of multiple targets or interferences within the auxiliary data set. Accounting for more than one target or interference greatly complicates the problem. Possible solutions include applying the NPIP algorithm to windows small enough that the existence of multiple interferences is not likely (i.e., apply it individually to the leading and lagging windows of auxiliary data) or performing a pre-detection screening of the data using a non-parametric test like the Page test described in [26] or by passing a small-window-NPIP over the time series and tagging all strong spatially compact interferences. These strong deviations from the background would then be excluded from use in the normalization process.

4

Instantaneous probability of false alarm

The primary goal of a normalization scheme is to provide a constant false alarm probability in the presence of a specific type of change in the null distribution, which, in this case, is the reverberation distribution. For example, the mean power level normalizers provide constant P_{fa} for any reverberation power level. There is, however, a price to be paid for this invariance. The variability of parameter estimation essentially introduces a variability on the threshold used for detection, changing both the detection and false alarm performance.

In this section, a new method for evaluating and comparing the false alarm performance of normalizers is proposed. Traditionally, normalizers are evaluated by their loss in detection performance when the detector thresholds are chosen to provide the same P_{fa}. However, when the auxiliary data are corrupted by interferences or if the thresholds are chosen based on incorrect assumptions about the reverberation statistics, the false alarm performance changes and should be considered separately and in addition to P_d. The method proposed in this section specifically considers the variability on the false alarm performance introduced by the estimation of reverberation parameters and provides an idea of what the detection performance will be. Detection performance is considered more fully in Section 5.

4.1 Mean power level normalizer

The effect of the variability of parameter estimation on the probability of false alarm for a mean level normalizer may be described by

$$\begin{aligned} P_{fa} &= \Pr_0\left\{\frac{X}{\sqrt{\hat{\lambda}}} > h\right\} \\ &= \mathrm{E}_{\hat{\lambda}}\left[\Pr_0\left\{X > h\sqrt{\hat{\lambda}} \,\middle|\, \hat{\lambda}\right\}\right] \\ &= \mathrm{E}_{\hat{\lambda}}\left[P_{fa}\left(\hat{\lambda}, h\right)\right] \end{aligned} \tag{36}$$

where h is a threshold chosen to provide a specified P_{fa}, the probability is taken under the null or reverberation-only hypothesis and the expectation is taken over

the reverberation power level estimate $\hat{\lambda}$. The quantity

$$\begin{aligned} P_{fa}\left(\hat{\lambda}, h\right) &= \Pr_0\left\{X > h\sqrt{\hat{\lambda}} \,\middle|\, \hat{\lambda}\right\} \\ &= 1 - F\left(h\sqrt{\hat{\lambda}}\,; \lambda\right) \end{aligned} \tag{37}$$

where $F(x;\lambda)$ is the CDF of X under the null hypothesis may be thought of as the conditional P_{fa} in a manner analogous to the conditional signal-to-noise ratio of Reed, Mallett and Brennan [27] or as the instantaneous P_{fa} in the sense that it is the P_{fa} given the current estimate of the reverberation power. The instantaneous P_{fa} provides a measure of the quality of the parameter estimation and an indication of the effect on detection performance, particularly in the presence of interferences in the auxiliary data window. As an example, consider Fig. 4 where the PDF of $\log_{10}\left(P_{fa}\left(\hat{\lambda}, h\right)\right)$ is shown for a cell-averaging constant false alarm rate detector (CA-CFAR), an order statistic constant false alarm rate detector (OS-CFAR), and a non-parametric interference pruning constant false alarm rate detector (NPIP-CFAR). The OS-CFAR detector used the 82^{nd} ordered statistic of the 100 samples of Rayleigh distributed auxiliary data. The NPIP-CFAR detector removed auxiliary data potentially corrupted by a target or target-like interference by assuming a maximum of $m_{\max} = 10$ target samples and using thresholds generated according to eq. (34) with $\alpha = 0.1$. The remaining data were then used in the manner of a CA-CFAR detector to estimate the reverberation power level. All of the detectors have their thresholds set so that $P_{fa} = 10^{-4}$, for which the NPIP-CFAR required simulation analysis. As expected, the PDFs of the instantaneous P_{fa} for the OS-CFAR and NPIP-CFAR have broader tails than those of the CA-CFAR detector indicating slightly worse performance. Note that the actual P_{fa} is the expected value of 10 raised to the random variable represented by the PDFs shown in the figures.

If parameter estimation were perfect, the PDF of the instantaneous P_{fa} would have an impulse function at the actual P_{fa} and the corresponding CDF would look like a rising step function with the transition at the P_{fa}. From this ideal, one could use the slope of the CDF of the instantaneous P_{fa} at the desired P_{fa} as a measure of effectiveness. The slope of the CDF is, of course, the PDF, and indicates the steepness of the CDF in the region of the P_{fa}—a steeper CDF at the mean implies less variance in the PDF and thus more precise false alarm performance. This was, in fact, how the 82^{nd} order statistic was chosen in the previous example, and it is clearly seen in Fig. 4 that the CA-CFAR has the largest PDF at the desired P_{fa}.

Introduction of a non-fluctuating (Swerling Type 0 resulting in Rician distributed data) target-like interference into 5 of the 100 samples of auxiliary data shifts all of the instantaneous P_{fa} PDFs to the left, as seen in Fig. 5, indicating a reduction in detection performance (target masking). The interference had an interference-to-reverberation power ratio (IRR) of 10 dB and was randomly positioned within

the auxiliary data for each of the 10,000 simulation trials. Clearly the PDF of the instantaneous P_{fa} for the NPIP-CFAR detector is affected the least of the three detectors, remaining largely unchanged from the case where no interference is present. As a smaller instantaneous P_{fa} implies a larger effective threshold and thus a smaller probability of detection, clearly the NPIP-CFAR detector provides the best performance in the presence of such an interference in the auxiliary data.

4.2 Statistical normalizer

The instantaneous P_{fa} may be similarly developed from the definition of the P_{fa} for the statistical normalizer of eq. (4)

$$\begin{aligned} P_{fa} &= \mathrm{Pr}_0\left\{g\left(X;\hat{\Theta}\right) > h\right\} \\ &= \mathrm{Pr}_0\left\{X > g^{-1}\left(h;\hat{\Theta}\right)\right\} \\ &= \mathrm{E}_{\hat{\Theta}}\left[\mathrm{Pr}_0\left\{X > g^{-1}\left(h;\hat{\Theta}\right)\middle|\hat{\Theta}\right\}\right] \\ &= \mathrm{E}_{\hat{\Theta}}\left[P_{fa}\left(\hat{\Theta},h\right)\right] \end{aligned} \tag{38}$$

where the dependence of g on $\hat{\Theta}$ has been indicated explicitly and g^{-1} is the functional inverse of g. The instantaneous P_{fa} is then

$$\begin{aligned} P_{fa}\left(\hat{\Theta},h\right) &= \mathrm{Pr}_0\left\{X > g^{-1}\left(h;\hat{\Theta}\right)\middle|\hat{\Theta}\right\} \\ &= 1 - F\left(g^{-1}\left(h;\hat{\Theta}\right);\Theta\right) \end{aligned} \tag{39}$$

where $F(x;\Theta)$ is the CDF of X under the null hypothesis.

The instantaneous P_{fa} provides a complete picture of the false alarm performance, with the average value representing the standard probability of a false alarm. In the presence of non-Rayleigh reverberation, the consequences of assuming Rayleigh reverberation or attempting to account for the departure from Rayleigh become evident in the PDF of the instantaneous P_{fa} as do the effects of target masking and false alarm rate inflation.

4.3 Statistical normalizer: Weibull reverberation

If X is Weibull distributed with parameters $\Theta = (\alpha,\ \beta)$ and g is as in eq. (10) with the parameter estimates $\hat{\Theta} = \left(\hat{\alpha},\ \hat{\beta}\right)$, the instantaneous P_{fa} is

$$P_{fa}\left(\hat{\Theta},h\right) = \exp\left\{-\alpha\left(\frac{h^2}{\hat{\alpha}}\right)^{\frac{\beta}{\hat{\beta}}}\right\}. \tag{40}$$

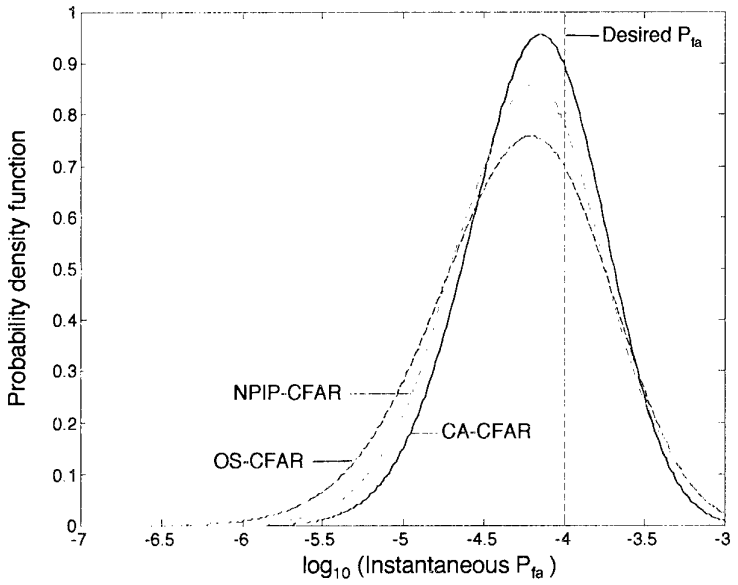

Figure 4 *Probability density function of* $\log_{10}$ *of instantaneous* P_{fa} *for CA-CFAR, OS-CFAR, and NPIP-CFAR with* 100 *samples of Rayleigh distributed auxiliary data. The thresholds for each detector were chosen so that the average* $P_{fa} = 10^{-4}$.

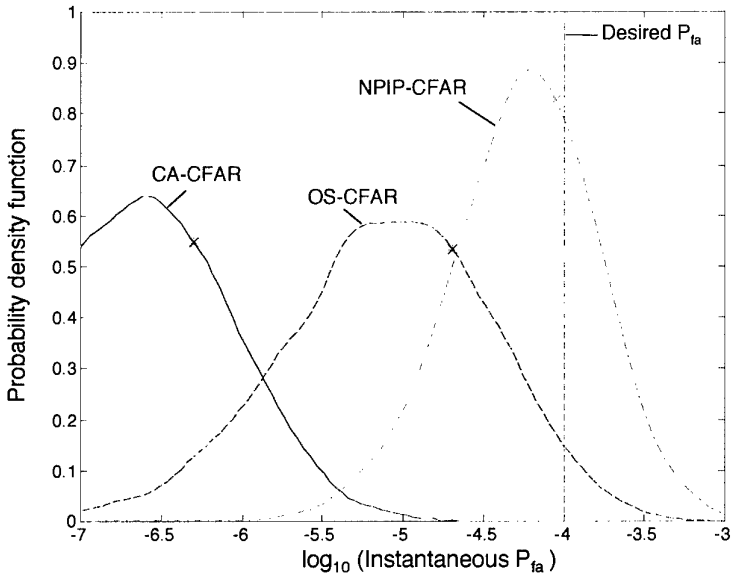

Figure 5 *Same as the above figure except with a* 10 *dB IRR non-fluctuating target corrupting 5 samples of the auxiliary data. The actual* P_{fa} *is indicated on each curve by an* $*$.

If the parameters are estimated perfectly (i.e., $\hat{\Theta} = \Theta$), the instantaneous P_{fa} becomes constant at $P_{fa}(h) = \exp\{-h^2\}$, exactly that for the Rayleigh distribution.

In [6] the maximum likelihood (ML) estimators for the Weibull parameters had less error between the parameter estimate generated CDF and the actual CDF but did not fit the sample CDF as well as the method of moments (MM) estimators for moderate kurtosis values. The instantaneous P_{fa} provides a means for comparing the performance of these estimators in a statistical normalizer with the CA-CFAR normalizer using a measure relevant to detector performance. The PDFs of $\log_{10}\left(P_{fa}\left(\hat{\Theta}, h\right)\right)$ of eq. (40) for the statistical normalizer using the ML and MM parameter estimators and for the CA-CFAR detector are shown in Fig. 6. The PDFs are estimated from 10,000 simulation trials with Weibull distributed reverberation when the power and kurtosis are both 1 ($\alpha = 1.1003$ and $\beta = 1.6147$). The thresholds for all of the detectors were chosen assuming Rayleigh distributed reverberation (i.e., $h = \sqrt{-\log P_{fa}}$). The PDFs of the instantaneous P_{fa} for the statistical normalizers using the ML and MM parameter estimates are nearly indistinguishable and clearly provide better performance than the CA-CFAR detector which blindly assumes the data to be Rayleigh. Improved false alarm performance is illustrated by the decreasing variance and trend of the mean toward the desired P_{fa} as more data are used to estimate the Weibull parameters.

The actual P_{fa} and the standard deviation of the instantaneous P_{fa} are shown in Table 1 where it is seen that the MM parameter estimates provide slightly, though not significantly, better performance for these particular α and β. Increasing the kurtosis resulted in identical performance for the detector using the ML parameter estimates and slightly worse performance for the detector using the MM parameter estimates. The equivalence of the performance over varying α and β for the detector using the ML parameter estimates indicates that there may be an invariance to these parameters, providing a constant false alarm rate over the complete Weibull family of distributions. This invariance does in fact exist when the ML parameter estimates are used in either the nonlinearity of eq. (10) or the instantaneous P_{fa} of eq. (40) as shown in Annex D. The importance of this result is that if the reverberation is truly Weibull distributed, then the false alarm performance of the statistical normalizer using the ML parameter estimates and the non-linearity of eq. (10) is constant regardless of the values of α and β. Thus, the threshold h may be chosen solely as a function of the desired P_{fa} and the amount of auxiliary data used to estimate the parameters of the Weibull distribution. As previously indicated, the detector using the MM parameter estimates does not enjoy this freedom. Unfortunately, the lack of a closed form solution for the ML estimates of α and β precludes an exact analytical analysis of the false alarm performance, thus forcing the use of simulation. The invariance of the nonlinearity of eq. (10) to changes in α and β provides a strong argument for using the ML parameter estimators over the MM estimators, even though they may be slightly more computationally intensive. Goldstein [28] has also proposed a detector having invariant false alarm performance over the family of

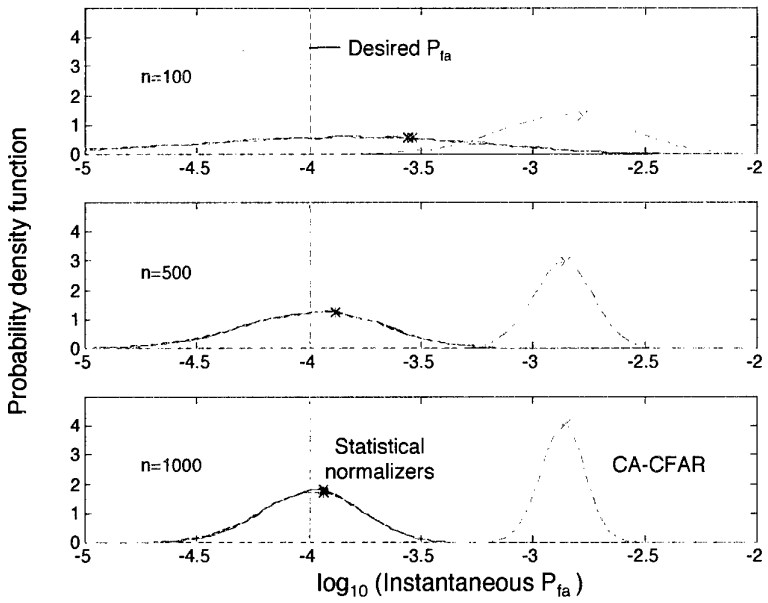

Figure 6 *Probability density function of* $\log_{10}$ *of instantaneous* P_{fa} *for statistical normalizers using ML and MM parameter estimates, which are nearly identical, and for CA-CFAR detector with* 100, 500 *and* 1000 *samples of Weibull distributed auxiliary data. The actual* P_{fa} *for each detector is indicated by the* $*$.

Weibull distributions, though it does not have the maximum likelihood parameter estimation argument that supports the statistical normalizer.

Table 1 *Mean (P_{fa}) and standard deviation of instantaneous P_{fa} for ML and MM parameter estimates of Weibull distributed reverberation using auxiliary data sets of size $n = 100$, 500 and 1000.*

	ML Estimator		MM Estimator	
n	P_{fa}	$\text{std}\left[P_{fa}\left(\hat{\Theta}, h\right)\right]$	P_{fa}	$\text{std}\left[P_{fa}\left(\hat{\Theta}, h\right)\right]$
100	2.873E-4	4.830E-4	2.751E-4	4.744E-4
500	1.286E-4	0.961E-4	1.280E-4	0.985E-4
1000	1.141E-4	0.582E-4	1.138E-4	0.596E-4

The false alarm performance of the statistical normalizer assuming Weibull reverberation in the presence of a target-like interference is examined in Figs. 7 and 8. The PDF of $\log_{10}\left(P_{fa}\left(\hat{\Theta}, h\right)\right)$ of eq. (40) using the ML parameter estimates is shown for the statistical normalizer with and without target pruning. Figure 7 represents the case of $n = 100$ auxiliary data samples and Fig. 8 when $n = 500$ samples are used. Both have 5 auxiliary data samples corrupted by a non-fluctuating (see eq. (16)) interference with the indicated interference-to-reverberation ratio (IRR) and the remaining samples unit power Rayleigh distributed. The target samples were inserted adjacent to each other with the position chosen randomly for each of the 10,000 trials. The target pruning algorithm assumed a maximum of $m_{\max} = 10$ target samples when $n = 100$ and $m_{\max} = 20$ when $n = 500$ and used thresholds generated according to eq. (34) with $\alpha = 0.1$. The PDF of the conditional P_{fa} when there is no interference present is either the upper ($n = 100$) or middle ($n = 500$) graph of Fig. 6. As the IRR increases, the PDF of the conditional P_{fa} and its mean for the normalizer without target pruning shifts far to the left of the desired $P_{fa} = 10^{-4}$, indicating much higher effective thresholds and a reduced detection performance. When target pruning is employed, the P_{fa} does not change substantially, though the conditional P_{fa} indicates that a slight reduction in detection performance will still be observed as there is more mass in the PDF at lower values.

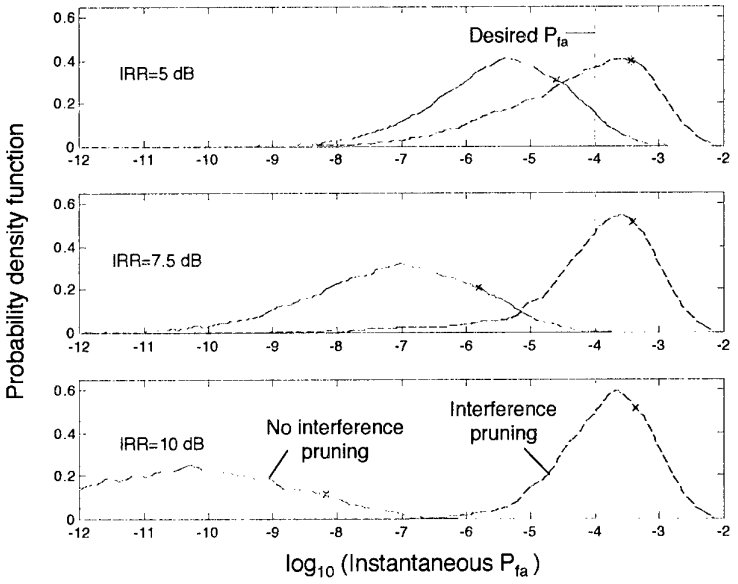

Figure 7 *Probability density function of* $\log_{10}$ *of instantaneous* P_{fa} *for statistical normalizer with ML parameter estimator with and without NPIP for varying IRR. Auxiliary data consisted of* 100 *samples of Rayleigh data,* 5 *of which were corrupted by non-fluctuating interference. The actual* P_{fa} *for each detector is indicated by the* $*$.

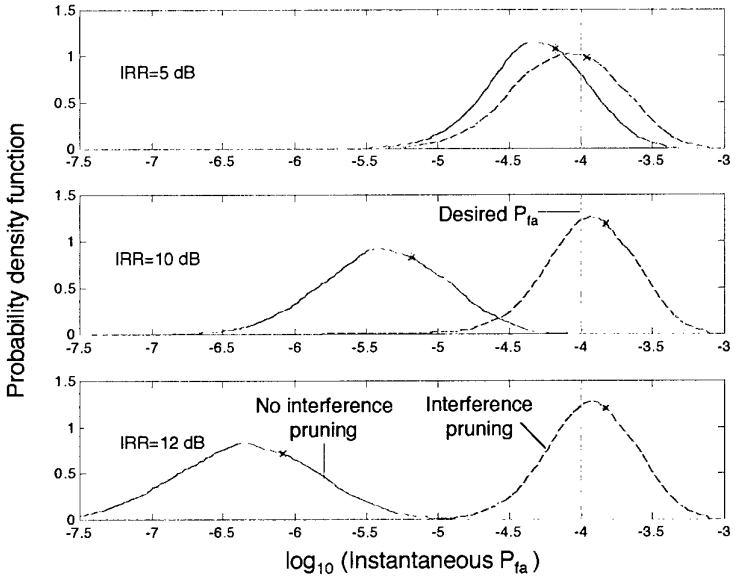

Figure 8 *Same as the above figure except with* 500 *samples of auxiliary data.*

4.4 Statistical normalizer: Rayleigh mixture reverberation

If the reverberation amplitude data sample X is distributed according to a Rayleigh mixture with parameters $\Theta = [\pi_1 \ \cdots \ \pi_p \ \lambda_1 \ \cdots \ \lambda_p]$ and g is as in eq. (14) with the parameter estimates $\hat{\Theta} = \left[\hat{\pi}_1 \ \cdots \ \hat{\pi}_p \ \hat{\lambda}_1 \ \cdots \ \hat{\lambda}_p\right]$, then the instantaneous P_{fa} is

$$P_{fa}\left(\hat{\Theta}, h\right) = \sum_{i=1}^{p} \pi_i \exp\left\{-\frac{1}{\lambda_i}\left[g^{-1}\left(h; \hat{\Theta}\right)\right]^2\right\} \tag{41}$$

where $g^{-1}\left(h; \hat{\Theta}\right)$ is the functional inverse of g, which does not have an analytical solution when there are two or more components in the mixture with different powers. If the maximum likelihood estimates for the mixture proportions and powers are obtained via the EM algorithm described in Section 2.2.2, then the false alarm performance is scale invariant; that is, if the power of the reverberation data changes, the function $g\left(x; \hat{\Theta}\right)$, the instantaneous P_{fa} and the P_{fa} do not change[1].

In order to examine the performance of the statistical normalizer in realistic reverberation, the Rayleigh mixture parameters are estimated from the SCARAB data used to create the P_{fa} estimates of Fig. 1 and data from one of SACLANT Undersea Research Centre's SWAC sea-trials. In both cases, the data were well fit by a three component Rayleigh mixture with the proportions and powers as noted in Table 2 for the SWAC data and Table 3 for the SCARAB data. Note that these SWAC data may also be adequately fit by a two component Rayleigh mixture. An indication of the severity of non-Rayleighness of these distributions is seen in the (β_2, β_1) plots found in Fig. 9. This type of plot shows the departure of the third and fourth order moments (skewness and kurtosis) from that of the Rayleigh distribution (see [6] for further information). Though both the reverberation models exhibit non-Rayleigh character, the SCARAB data model is extremely non-Rayleigh as evidenced by the large values of both skewness and kurtosis.

The PDF of $\log_{10}$ of the instantaneous P_{fa} for the CA-CFAR and statistical normalizers is shown in Fig. 10 for both reverberation models when the desired P_{fa} is 10^{-4}. Clearly, use of the CA-CFAR produces a substantially larger P_{fa}. The statistical normalizer brings the P_{fa} closer to the design value at the expense of an increase in the variance of the $\log_{10}$ of the instantaneous P_{fa}. As expected, the false alarm performance of the statistical normalizer becomes closer to the desired performance as more data is used to estimate the Rayleigh mixture parameters. That the statistical normalizer is not invariant to changes in the mixture parameters is seen in the difference in performance between the SWAC and SCARAB data models. The

[1] This may be proven by first showing that the EM algorithm estimates of the mixture proportions $\{\hat{\pi}_i\}$ are not affected at all by a change in scale and then noting the dependence of $g\left(x; \hat{\Theta}\right)$ on the ratio $\frac{x^2}{\lambda_i}$ which becomes distributionally free from any scale applied to the data.

less extreme reverberation from the SWAC data model is easily normalized by using 500 samples of auxiliary data while the SCARAB data requires more than twice as much to provide equivalent control over the false alarm performance.

Figures 11 and 12 illustrate how the false alarm performance degrades when an interference 5 samples long is introduced into the auxiliary data if the NPIP algorithm is not first used to identify spatially compact interference and then remove it. When the NPIP algorithm is not used, the probability of false alarm is substantially lower, indicating target masking and a loss in detection performance. Use of the NPIP algorithm results in minimal change in performance.

The results shown in Fig. 11 used 100 samples of auxiliary data while the results of Fig. 12 used 500 samples. The number of order statistics used in the NPIP algorithm ($m_{\max}$) must be adjusted according to the amount of auxiliary data; in particular, $m_{\max}$ must be increased when more auxiliary data are used. This may be explained by the occurrence of a greater number of reverberation data that exceed the interference data values, thus requiring consideration of a larger number of the higher order statistics to guarantee capturing interference. In the simulations performed for this report, $m_{\max} = 10$ when $n = 100$ samples of auxiliary data were used and $m_{\max} = 20$ when $n = 500$ samples were used.

Table 2 *Mixture proportions and powers estimated from SWAC data.*

Proportion	Power
0.5958	1.5529
0.3288	0.2262
0.0754	0.0053

Table 3 *Mixture proportions and powers estimated from SCARAB data.*

Proportion	Power
0.4290	0.9500
0.4241	0.6050
0.1469	2.2863

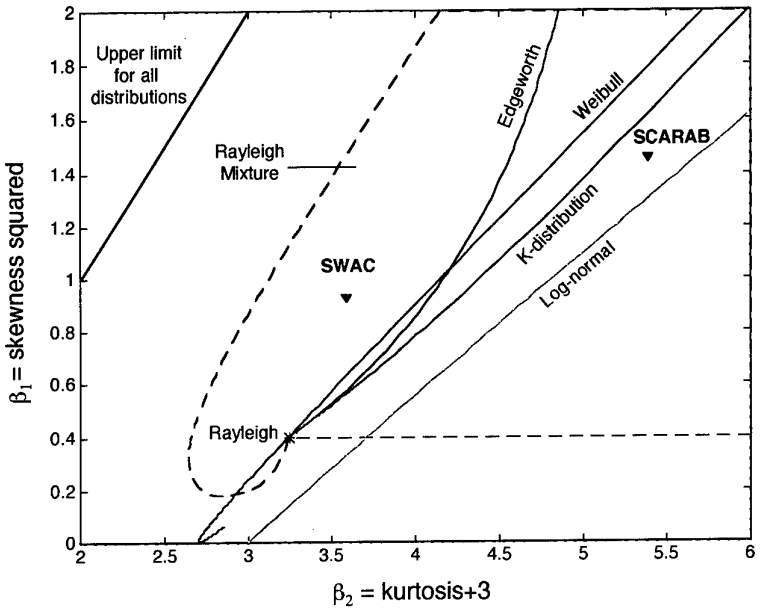

Figure 9 *Skewness and kurtosis plotted on a (β_2, β_1) plane for the Rayleigh mixture models estimated from the SWAC and SCARAB reverberation data. Note the extremity of the SCARAB Rayleigh mixture model.*

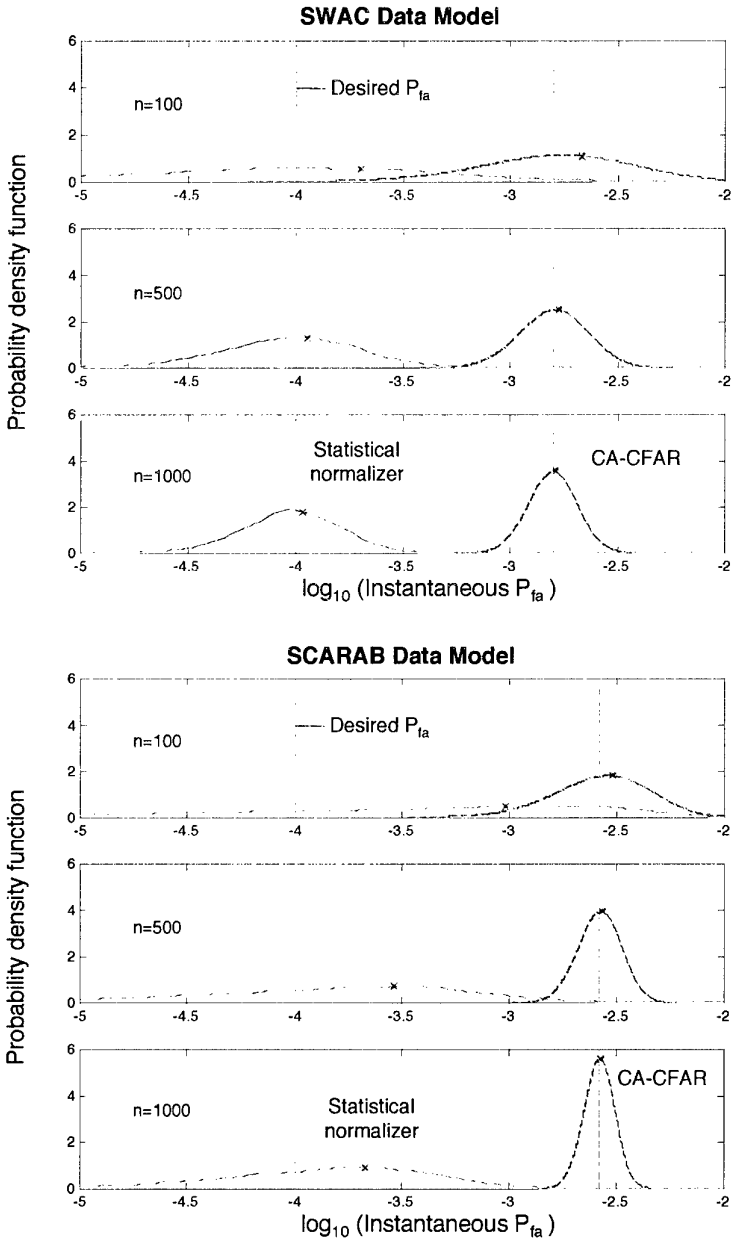

Figure 10 *Probability density function of* $\log_{10}$ *of instantaneous* P_{fa} *for statistical normalizer and CA-CFAR detectors with* 100, 500 *and* 1000 *samples of Rayleigh mixture distributed auxiliary data. The actual* P_{fa} *for each detector is indicated by the* $*$.

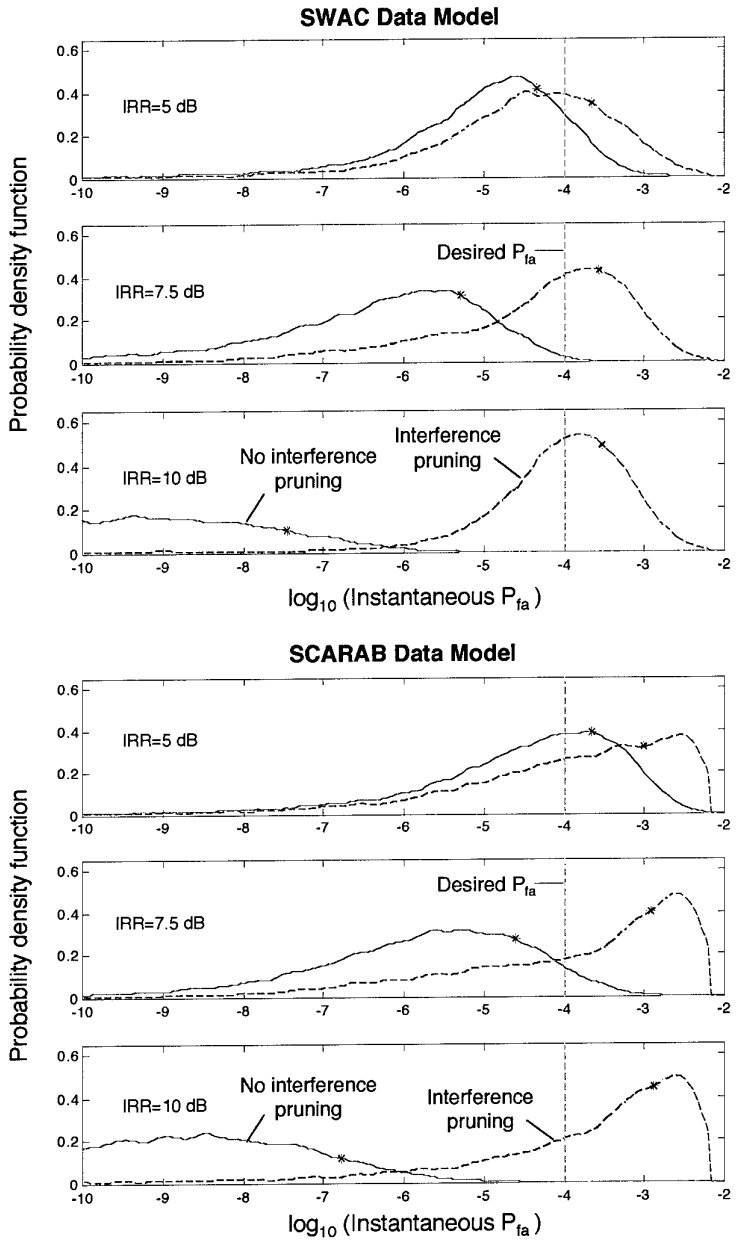

Figure 11 *Probability density function of* $\log_{10}$ *of instantaneous* P_{fa} *for statistical normalizers with and without NPIP for varying IRR. Auxiliary data consisted of* 100 *samples of Rayleigh mixture data,* 5 *of which were corrupted by a non-fluctuating interference. The NPIP assumed a maximum of* 10 *corrupted samples. The actual* P_{fa} *for each detector is indicated by the* $*$.

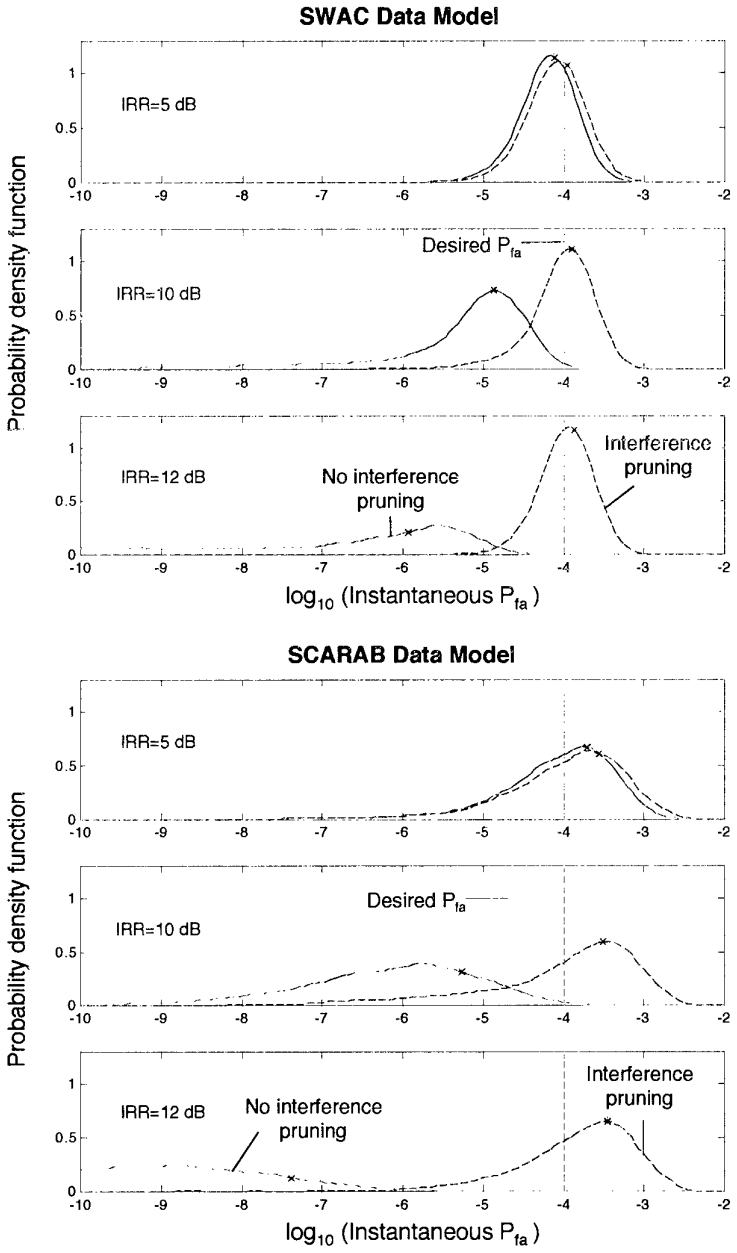

Figure 12 *Probability density function of* $\log_{10}$ *of instantaneous* P_{fa} *for statistical normalizers with and without NPIP for varying IRR. Auxiliary data consisted of* 500 *samples of Rayleigh mixture data,* 5 *of which were corrupted by a non-fluctuating interference. The NPIP assumed a maximum of* 20 *corrupted samples. The actual* P_{fa} *for each detector is indicated by the* $*$.

5
Detection performance

Detection performance depends directly on the type of detector used and the statistical characterization of the reverberation and target echo. To understand the relationships between detection and false alarm performance in the presence of non-Rayleigh reverberation, first assume that the distribution of the reverberation is known completely and that a simple threshold crossing detector is utilized; that is, a detection is declared when the matched filter output exceeds a certain level. The theoretical receiver operating characteristic (ROC) curve for detecting a non-fluctuating or Swerling Type 0 target in Rayleigh and non-Rayleigh reverberation with such a detector is shown in Fig. 13. The non-Rayleigh reverberation has the same power level as the Rayleigh reverberation (thus the signal-to-reverberation power ratio is the same for both curves) and is in the form of a Rayleigh mixture distribution with the parameters as found in Table 2. If the desired P_{fa} is 10^{-4}, the P_d is above 0.9 for Rayleigh reverberation. However, if the data are non-Rayleigh (with the distribution previously described) and a perfect mean power level normalizer is used, P_{fa} increases by over an order of magnitude and P_d increases very slightly (owing to the heavier tails of the reverberation), as illustrated in Fig. 13. The objective of the statistical normalizer is to account for the distribution of the reverberation, essentially moving along the dashed curve down to the point of the desired P_{fa}. The ensuing loss in P_d represents the cost of controlling the false alarms. It should be noted, however, that these curves assume identical signal-to-reverberation power ratios (SRRs). This may not be the case in practice; for example, increasing bandwidth reduces the range-bearing resolution cell size, potentially creating non-Rayleigh reverberation, but also reducing the reverberation power level (and possibly the target echo level) resulting in a different SRR. Fundamentally, when the reverberation distribution is known, the detector in the non-Rayleigh reverberation must operate somewhere on the dashed curve.

When the reverberation distribution is not known exactly, it must be modeled using an appropriate statistical distribution whose parameters are then estimated. This leads to sources of errors: mismatch between the actual reverberation distribution and the assumed one and losses associated with the estimation of the parameters characterizing the reverberation model. Choosing a very general model, such as a Rayleigh mixture, results in concentrating the losses to the parameter estimation. Choosing a specific model, such as the Weibull distribution, may lead to substantial mismatch losses.

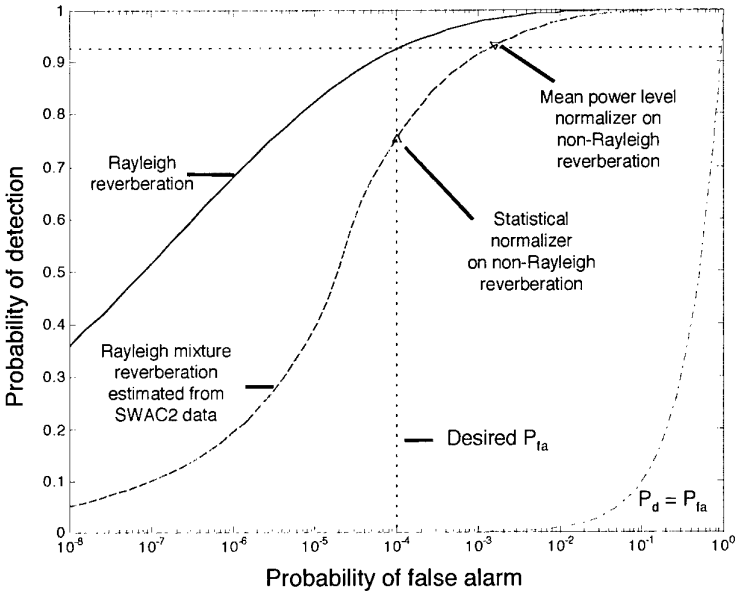

Figure 13 *ROC curve for non-fluctuating target in Rayleigh and non-Rayleigh reverberation.*

The conditional P_{fa} developed in the previous section provides a technique for examining the effects of parameter estimation and the losses expected from distributional mismatch. Given enough stationary real reverberation data is should also be feasible to evaluate the conditional P_{fa} for different models by using a sample CDF in place of $F(x;\Theta)$ in eq. (39). The conditional P_{fa} can also provide an indication of detection performance in that a decrease in performance is expected when there is a high probability of observing values of the instantaneous P_{fa} much lower than the desired P_{fa}. This, however, is not concrete enough to indicate good or bad performance.

The remainder of this section will illustrate through simulation that it is feasible to obtain detection performance near the dashed curve of Fig. 13 by using the statistical normalizer of Section 2 and the NPIP algorithm of Section 3. As an example, consider a non-fluctuating target occupying 5 adjacent range samples and auxiliary data consisting of a window 100 samples long. The detector in this case simply compares the largest value of the target bins to a threshold. The probability of detection for such a detector is shown as a function of the SRR in Fig. 14 when the reverberation is Rayleigh distributed and non-Rayleigh using the Rayleigh mixture of Table 2. Note that the ordinate has been plotted using the standard normal probability scale to expand the regions near zero and one. The threshold for each situation is chosen so that $P_{fa} = 0.01$ when the reverberation is Rayleigh, as is re-

flected in the curves for Rayleigh reverberation and Rayleigh mixture reverberation where the statistical normalizer is applied with perfect knowledge of the reverberation PDF. It can be seen from these curves that the desired P_{fa} is achieved by the tendency of P_d towards this value as SRR decreases. When the statistical normalizer is not used (i.e., assuming the reverberation is Rayleigh) when the reverberation is non-Rayleigh, P_{fa} exceeds the desired value along with an increase in P_d. The 'x' ($n = 100$) and 'o' ($n = 500$) marked simulation results were for clean auxiliary data windows; that is, the data were all distributed according to the Rayleigh mixture of Table 2. These curves illustrate that increasing the amount of auxiliary data used to estimate the reverberation PDF parameters allows achieving performance near that when the PDF is known exactly. The '+' marked simulation results placed a 10 dB SRR, 5 range sample, non-fluctuating interference in the middle of the auxiliary data ($n = 100$), resulting in a Rician mixture for those samples. Here it is seen that P_d is slightly below the performance when no interference exists, indicating that the NPIP algorithm removed most of, but not all of, the interfering signal from the auxiliary data. These results indicate that performance near the expected theoretical values can be achieved even in the presence of interferences by using the NPIP algorithm in conjunction with a statistical normalizer, with improving performance as more auxiliary data are used.

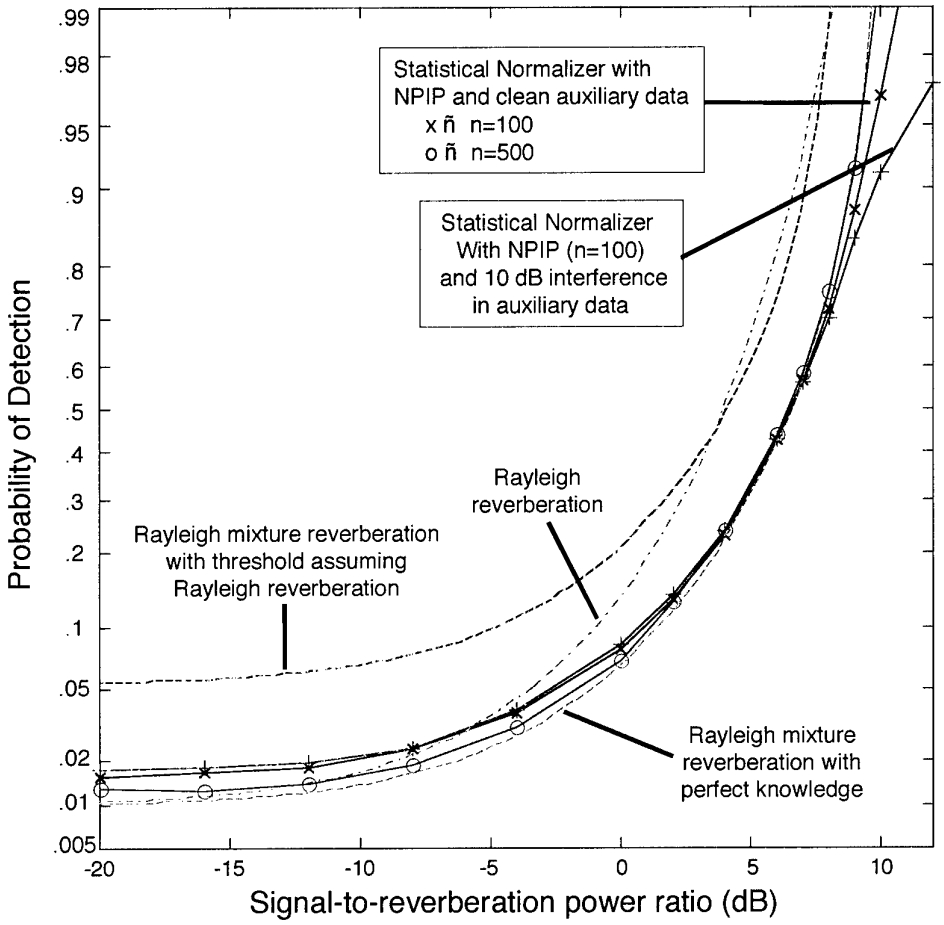

Figure 14 *Probability of detection as a function of signal-to-reverberation power ratio for a 5 sample target with a detector comparing the maximum over the target cells to a threshold. The thresholds were chosen to provide a false alarm probability of* 0.01. *The statistical normalizer used the NPIP algorithm to remove any interference present in the auxiliary data prior to estimating the parameters of a three component Rayleigh mixture. The 'x' ($n = 100$) and 'o' ($n = 500$) marked simulations were for clean auxiliary data; that is, auxiliary data with no interference present. The '+' ($n = 100$) marked simulation had auxiliary data contaminated by a 10 dB SRR, 5 range sample, non-fluctuating interference.*

6

Application to real data

6.1 Experiment and sonar configuration

The data analyzed in this report were collected during SACLANT Undersea Research Centre's SCARAB '97 sea-trial, which took place in the area north of the island of Elba off the coast of Italy. Reverberation data were collected using a high power towed source and the Centre's low frequency towed line array. A 2 second linear frequency modulated (LFM) waveform sweeping from 450 to 700 Hz was transmitted from the source, which was towed at approximately 62 meters depth and was comprised of three transducers spaced approximately 1.5 meters apart and beamformed to point 40 degrees down from horizontal. The hydrophone data were received from 128 sensors spaced 0.5 meters apart and were beamformed using Hanning shading on the array to beams spaced so that their beampatterns overlapped 3dB down from the main response axis at 900 Hz, resulting in 54 beams spanning from forward to aft endfire. The correspondence between beam number and main response axis angle is depicted in Fig. 15 where zero degrees indicates forward endfire. The data from each beam were matched filtered, basebanded so that the center of the waveform band (575 Hz) shifted to zero Hertz, and decimated to a sampling frequency of 250 Hz. The resulting data are approximately statistically independent from sample to sample in range and provide a range sampling interval of 3 meters assuming 750 m/s for the two-way speed of sound.

6.2 Single beam analysis

One of the beams containing non-Rayleigh reverberation is chosen for more detailed examination. The matched filtered beam output is mean power level normalized using a trimmed mean order statistic CFAR processor [2] with leading and lagging windows each containing 75 samples with a buffer of 2 samples surrounding the range cell being processed. The order statistic CFAR processor trimmed the upper and lower 10% of the combined leading and lagging windows of auxiliary data. The configuration of the normalizer window that is slid along the matched filtered beam output is illustrated in Fig. 16.

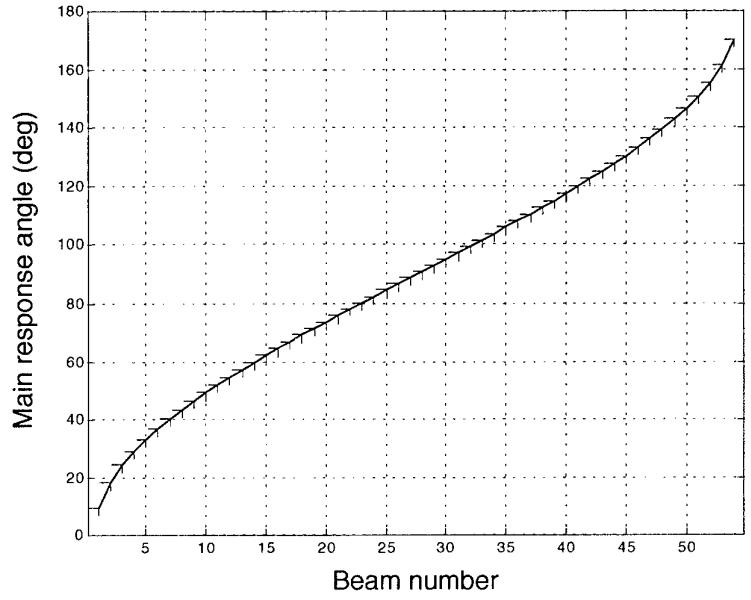

Figure 15 *Beamformer main response axis angles as a function of beam number.*

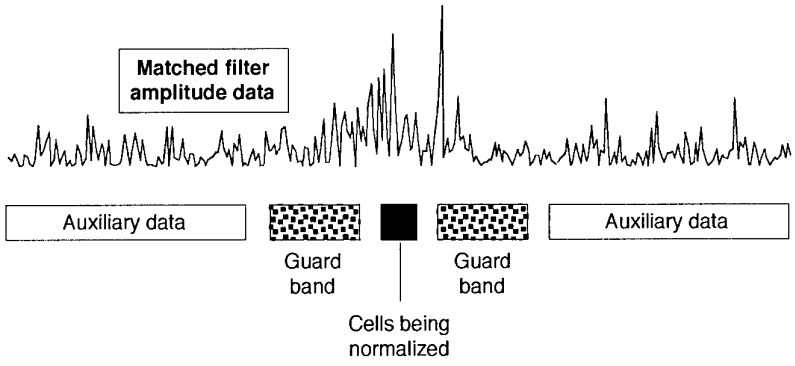

Figure 16 *Normalizer configuration.*

6.2.1 Distributional models

The parameters for the non-Rayleigh models described in [6] are estimated and used to generate frequency curves (CDFs formed by using estimated rather than exact parameter values), from which the probability of false alarm is obtained, as shown in Fig. 17. Of all the models, the three component Rayleigh mixture model best fits the data as seen in Fig. 17 and further supported by the p-values of the Kolmogorov Smirnov (KS) test statistics between the models and the data found in Table 4 (a p-value near one indicates a good fit).

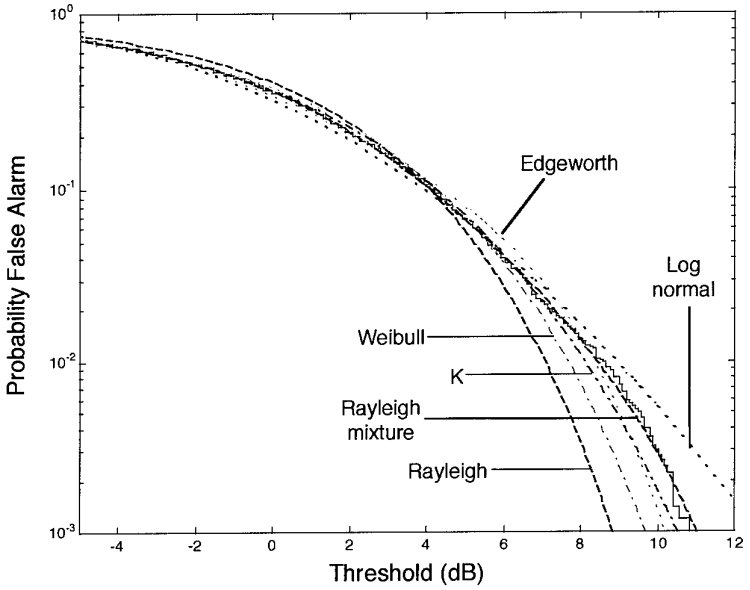

Figure 17 *Estimated and modeled P_{fa} for 5000 samples of data from the middle region of beam 37. The Rayleigh mixture (3 component) best fits the data.*

Table 4 *KS p-values for various non-Rayleigh reverberation models with data from middle region of beam 37.*

Model	KS p-value
Rayleigh	2.4e-14
Log-normal	3.3e-11
Edgeworth	0.0014
Weibull	0.0082
K	0.3204
Rayleigh mixture	0.9896

6.2.2 Statistical normalization

Statistical normalizers assuming either Weibull or Rayleigh mixture reverberation are then applied to the mean power level normalizer output under the assumption that the non-Rayleigh character of the reverberation is stationary over longer ranges than the reverberation power level. The statistical normalizers are implemented using leading and lagging windows each containing 250 samples with a buffer of 3 samples to either side of a target assumed to be 5 samples wide in the same configuration as that shown in Fig. 16. To decrease the amount of time required for processing, the same nonlinearity is applied to all 5 of the assumed target samples. The statistical normalizer assuming Rayleigh mixture reverberation always used three components and was initialized by the most previous mixture parameter estimates unless one of the mixture proportions or powers was near zero; that is, if the reverberation were well fit by fewer than three mixture components. The data are displayed in Fig. 18 along with the threshold that produces $P_{fa} = 10^{-4}$ in unit power Rayleigh reverberation. Clearly the statistical normalizer using the Rayleigh mixture model has the fewest threshold crossings (false alarms).

The (β_2, β_1) measures of the skewness and kurtosis [6] are estimated from overlapping blocks of 1000 data samples for the mean power level normalizer and the statistical normalizers assuming Weibull or three component Rayleigh mixture reverberation. Figure 19 illustrates how non-Rayleigh the mean power level normalizer data are, and that the statistical normalizer using a three component Rayleigh mixture controls the skewness and kurtosis well.

The P_{fa} estimated from the mean power level normalizer and the statistical normalizers assuming Weibull or three component Rayleigh mixture reverberation is shown in Fig. 20. Observe that the statistical normalizer data are not exactly Rayleigh, though their false alarm performance is closer to the desired value than that of the mean power level normalizer. Were the reverberation not as extremely non-Rayleigh as it is, as discussed in Section 4.4, the false alarm performance of the statistical normalizer with the Rayleigh mixture model would be closer to the desired Rayleigh reverberation curve.

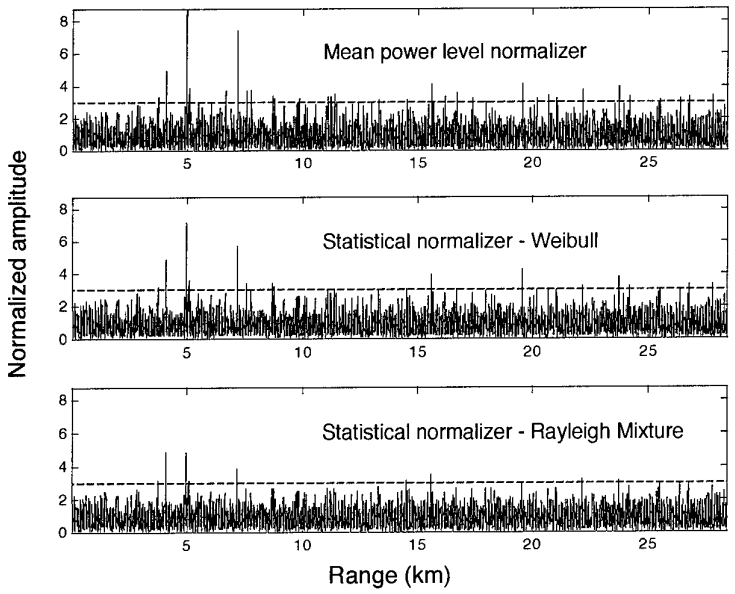

Figure 18 *Normalized data for beam 37. The dashed line represents the threshold for which the P_{fa} for a Rayleigh random variable is 10^{-4}.*

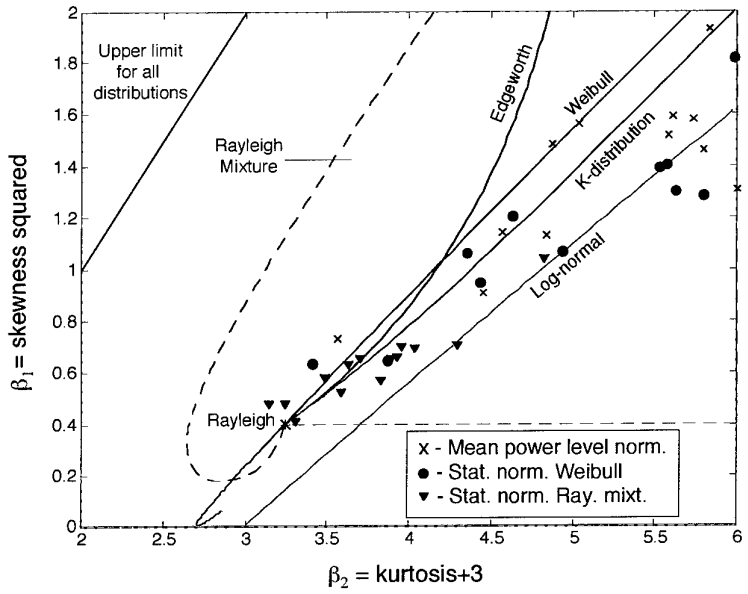

Figure 19 *(β_2, β_1) estimates for mean power level normalizer and statistical normalizers assuming Weibull and Rayleigh mixture reverberation. The estimates were formed using blocks 1000 samples long from the data in beam 37 overlapping 50%.*

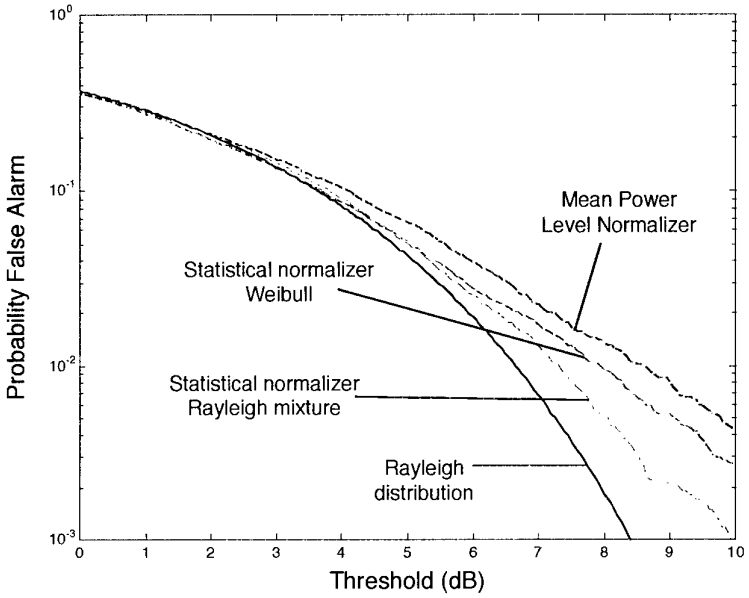

Figure 20 *P_{fa} estimated from beam 37 (approx. 10,000 samples) for mean power level normalizer and statistical normalizers assuming Weibull and Rayleigh mixture reverberation.*

6.3 Full beam analysis

Images of all the beams from one ping of data are shown in Fig. 21 in a rectangular range-beam grid for the mean power level normalizer and the statistical normalizer using a three component Rayleigh mixture as described in Section 6.2.2. The bright areas visible in the mean power level normalizer image around beams 10 and 35 are much less visible in the statistical normalizer image. Though not shown, the image for the statistical normalizer assuming Weibull reverberation did not clean up the non-Rayleigh reverberation as well as the statistical normalizer using the Rayleigh mixture model.

To provide a quantitative measure of the performance of the statistical normalizer, the p-value of the Kolmogorov-Smirnov (KS) test statistic between the observed data (blocks of 500 samples with 90% overlap) and the Rayleigh distribution are formed and displayed as images in Fig. 22. When the KS statistic p-value is near zero (black on the images), the Rayleigh distribution is a poor fit to the observed data. Values that aren't small indicate that the data may be well fit by the Rayleigh distribution. For example, the non-Rayleighness of the direct blast (waveform transmission) is

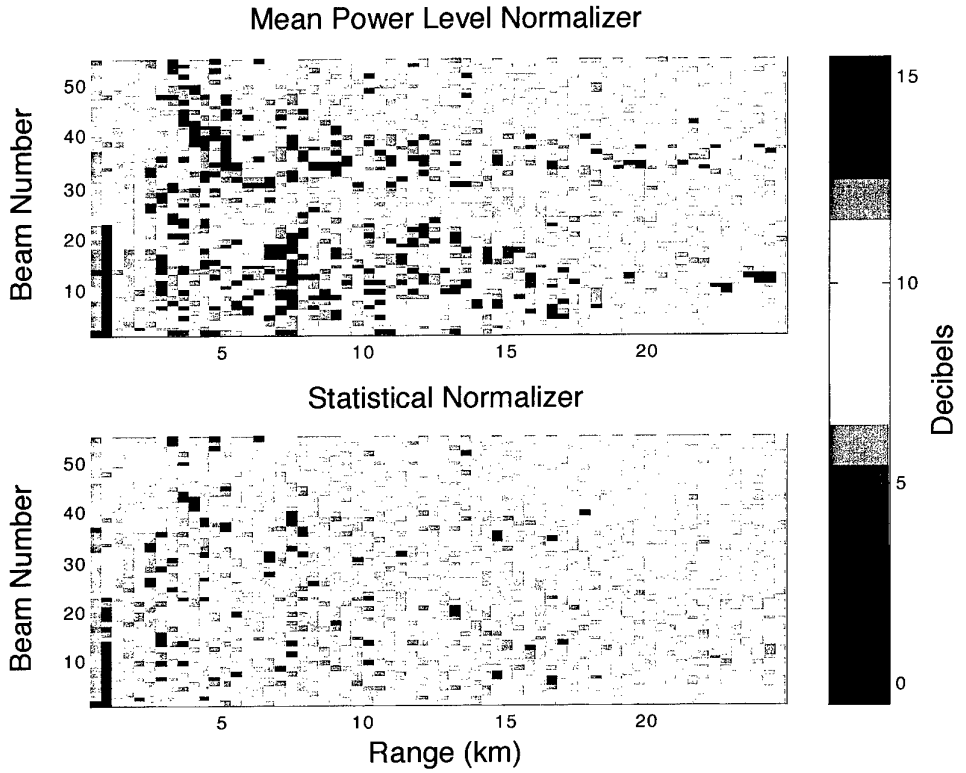

Figure 21 *Mean power level normalizer and statistical normalizer data using a three component Rayleigh mixture.*

clearly seen in the forward pointing beams (lower beam numbers) for all of the normalizers. The success of the statistical normalizer in converting the non-Rayleigh reverberation observed in the mean power level normalizer output is evident in the uniformity of the KS statistic p-values and their nearness to one. Both of these indicate that the statistical normalizer output data are closer than the mean power level normalizer data to the ideal: unit power Rayleigh reverberation across all beam and range cells where ever there is diffuse reverberation.

To determine how close the normalizer outputs are to this ideal, a similar field of Rayleigh reverberation was generated. The KS statistic p-values were then formed using the same block sizes and overlapping as for the normalizer data. Then, as the KS statistic p-values were themselves random variables, the CDF of the p-values was formed from the data beyond 4.5 km (some of the data nearer than 4.5 km are invalid owing to overloading of the receive array hydrophones by the transmission of other waveforms in the wavetrain). As seen in Fig. 23, the CDF of the KS statistic p-values for the mean power level normalizer indicates a much higher probability of observing non-Rayleigh reverberation (i.e., small KS statistic p-values). Application of a statistical normalizer assuming Weibull reverberation reduces this probability somewhat, but not as much as when the Rayleigh mixture model is used. The improvement is clearly indicated by the relative nearness of the Rayleigh mixture curve to that of the simulated Rayleigh data.

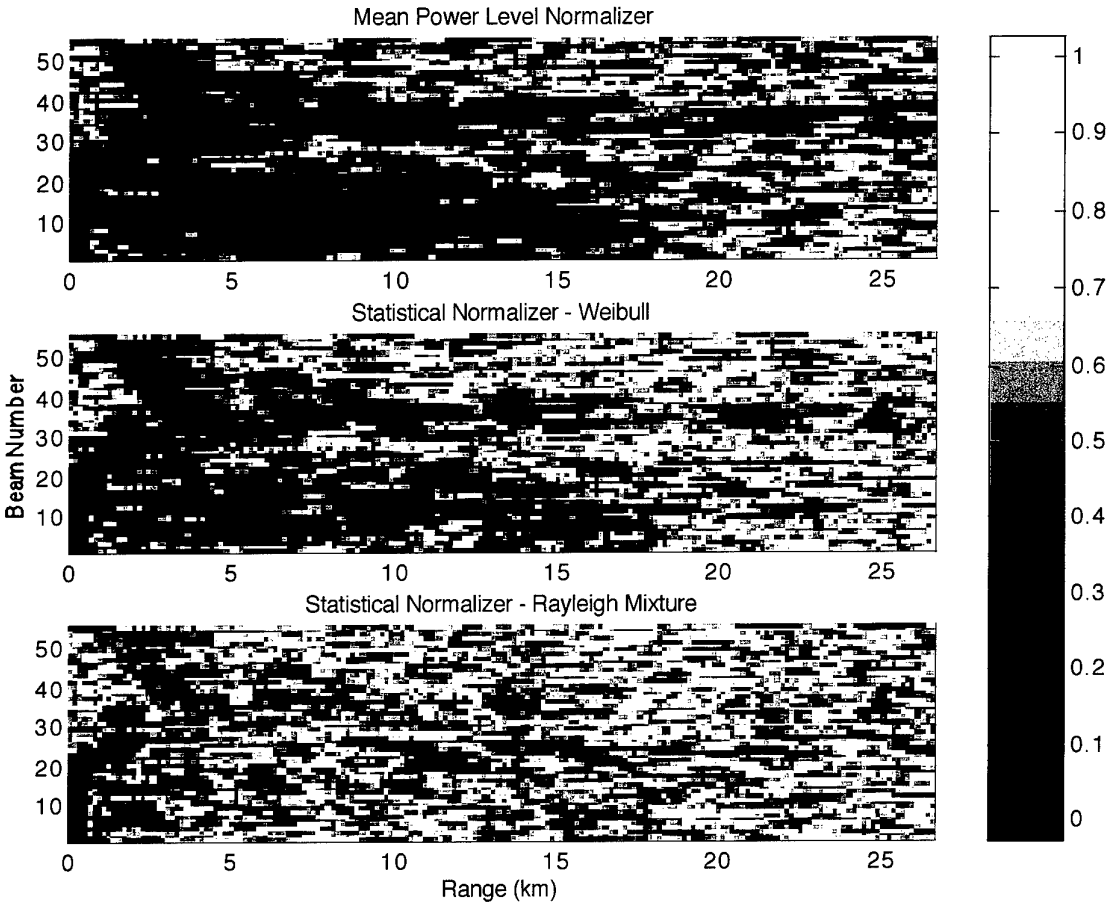

Figure 22 *KS statistic p-value between normalized data from one ping after mean power level normalization and statistical normalization assuming Weibull and three component Rayleigh mixture reverberation. Values near one more closely resemble the Rayleigh distribution.*

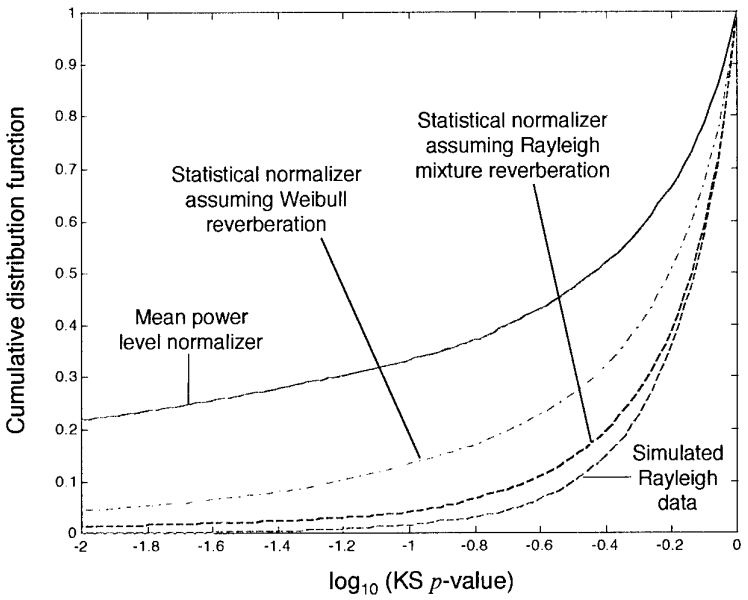

Figure 23 *Estimated CDF of the KS statistic p-values of Fig. 22 for data after the first* 4.5 *kilometers.*

7
Conclusion

Low frequency active sonar systems operating in shallow water have encountered non-Rayleigh reverberation, with the statistics changing in range and bearing. The lack of knowledge about the reverberation statistics and their non-stationarity hinders the application of automatic detection algorithms to range-bearing images exhibiting such non-Rayleigh reverberation. This report has presented a method for dealing with such reverberation by converting it back to the Rayleigh distribution through a tail de-emphasizing non-linearity. This algorithm, a statistical normalizer, was evaluated through simulation and then applied to real data. The simulation analysis indicated that the performance was linked to both the severity of the non-Rayleighness of the reverberation and the amount of data used to estimate the parameters of the reverberation model. Application to real data indicated that a large degree of the non-stationarity of the reverberation could be removed, producing range-bearing images suitable for multi-beam processing in the presence of non-Rayleigh reverberation.

In applying the statistical normalizer to real data, an algorithm was developed to prune strong, spatially compact interferences from auxiliary data that are subsequently used to estimate reverberation model parameters. The algorithm was based on the indices to the order statistics, and is therefore non-parametric (i.e., the performance is independent of the reverberation distribution) and applicable for use in reverberation following an unknown distribution.

In analyzing the false alarm performance of a simple threshold crossing detector operating on the statistical normalizer output, a new technique of examining the effect of parameter estimation was developed. The P_{fa} conditioned on the parameter estimate, called the conditional or instantaneous P_{fa}, was used to determine how variable the false alarm performance can be, illuminating the effect of interference corrupting auxiliary data and the effect of the statistical normalizer on non-Rayleigh reverberation.

The efficacy of the statistical normalizer in controlling the high and variable false alarm rates exhibited by non-Rayleigh reverberation regions observed in low-frequency active sonar, and the promising simulation results indicating acceptable detection performance lead to the recommendation that this algorithm be considered for inclusion in the Centre's real-time low-frequency active sonar system for use and the

eventual evaluation of larger data sets. At the same time, research should continue in developing reverberation models that well represent real data with a more parsimonious parameterization than the Rayleigh mixture model.

References

[1] J. T. Rickard and G. M. Dillard, "Adaptive detection algorithms for multiple-target situations," *IEEE Transactions on Aerospace and Electronic Systems*, vol. AES-13, no. 4, pp. 338–343, July 1977.

[2] P. P. Gandhi and S. A. Kassam, "Analysis of CFAR processors in nonhomogenous background," *IEEE Transactions on Aerospace and Electronic Systems*, vol. 24, no. 4, pp. 427–445, July 1988.

[3] C. Kim, D. Han, and H. Lee, "Generalized OS CFAR detector with noncoherent integration," *Signal Processing*, vol. 31, pp. 43–56, 1993.

[4] M. Lops and P. K. Willett, "L*l*-CFAR: A flexible and robust alternative," *IEEE Transactions on Aerospace and Electronic Systems*, vol. 30, no. 1, pp. 41–54, January 1994.

[5] X. Macé de Gastines, "Robust normalization algorithms for low-frequency active sonar signals," SR-244, SACLANT Undersea Research Centre, 1995.

[6] D. A. Abraham, "Modeling non-Rayleigh reverberation," SR-266, SACLANT Undersea Research Centre, May 1997.

[7] N. P. Chotiros *et al.*, "Acoustic backscattering at low grazing angles from the ocean bottom. Part II. Statistical characteristics of bottom backscatter at a shallow water site," *Journal of the Acoustical Society of America*, vol. 77, no. 3, pp. 975–982, March 1985.

[8] D. Marandino, "Low-frequency reverberation measurements with an activated towed array: Scattering strengths and statistics," SR-112, SACLANT Undersea Research Centre, 1987.

[9] M. Gensane, "A statistical study of acoustic signals backscattered from the sea bottom," *IEEE Journal of Oceanic Engineering*, vol. 14, no. 1, pp. 84–93, January 1989.

[10] S. Stanic and E. G. Kennedy, "Fluctuations of high-frequency shallow-water seafloor reverberation," *Journal of the Acoustical Society of America*, vol. 91, no. 4, pp. 1967–1973, April 1992.

[11] P. A. Crowther, *Fluctuation Statistics of Sea-bed Acoustic Backscatter*, pp. 609–622, Plenum, New York, 1980.

[12] S. T. McDaniel, "Seafloor reverberation fluctuations," *Journal of the Acoustical Society of America*, vol. 88, no. 3, pp. 1530–1535, September 1990.

[13] W. K. Stewart, D. Chu, S. Malik, S. Lerner, and H. Singh, "Quantitative seafloor characterization using a bathymetric sidescan sonar," *IEEE Journal of Oceanic Engineering*, vol. 19, no. 4, pp. 599–610, October 1994.

[14] V. V. Ol'shevskii, *Characteristics of Sea Reverberation*, Consultants Bureau, New York, 1967.

[15] A. P. Lyons, D. A. Abraham, T. Akal, and P. Guerrini, "Statistical evaluation of 80 kHz shallow-water seafloor reverberation," in *Proceedings of NATO SACLANT Undersea Research Centre Conference on High Frequency Acoustics in Shallow Water*, Lerici, Italy, July 1997, pp. 323–329.

[16] K. D. Ward, "Compound representation of high resolution sea clutter," *Electronics Letters*, vol. 17, no. 16, pp. 561–563, August 1981.

[17] S. A. Kassam, *Signal Detection in Non-Gaussian Noise*, Springer-Verlag, New York, 1988.

[18] D. M. Titterington, A. F. M. Smith, and U. E. Makov, *Statistical Analysis of Finite Mixture Distributions*, John Wiley & Sons, Inc., Chichester, 1985.

[19] G. V. Trunk, "Non-Rayleigh sea clutter: Properties and detection of targets," Report 7986, Naval Research Laboratory, 1976, Reprinted in *Automatic Detection and Radar Data Processing*, D. C. Schleher, Ed., Artech House, Dedham, 1980.

[20] A. P. Dempster, N. M. Laird, and D. B. Rubin, "Maximum likelihood from incomplete data via the EM algorithm," *Journal of the Royal Statistical Society, Series B*, vol. 2, pp. 1–38, 1977.

[21] R. A. Redner and H. F. Walker, "Mixture densities, maximum likelihood and the EM algorithm," *SIAM Review*, vol. 26, no. 2, April 1984.

[22] R. V. Hogg and A. T. Craig, *Introduction to Mathematical Statistics*, Macmillan Pub. Co., New York, fourth edition, 1978.

[23] H. Akaike, "A new look at the statistical model identification problem," *IEEE Transactions on Automatic Control*, pp. 716–723, December 1974.

[24] J. Rissanen, "Modeling by shortest data description," *Automatica*, pp. 465–471, September 1978.

[25] F. Palmieri and C. G. Boncelet, "L*l*-Filters—A new class of order statistic filters," *IEEE Transactions on Acoustics, Speech and Signal Processing*, vol. 37, no. 5, pp. 691–700, May 1989.

[26] D. A. Abraham, "A nonparametric Page test applied to active sonar detection," in *Proceedings of Oceans 96 Conference*, September 1996, pp. 908–913.

[27] I. S. Reed, J. D. Mallett, and L. E. Brennan, "Rapid convergence rate in adaptive arrays," *IEEE Transactions on Aerospace and Electronic Systems*, vol. AES-10, no. 6, pp. 853–863, November 1974.

[28] G. B. Goldstein, "False-alarm regulation in log-normal and Weibull clutter," *IEEE Transactions on Aerospace and Electronic Systems*, vol. AES-9, no. 1, pp. 84–92, January 1973.

[29] L. Råde and B. Westergren, *Beta β Mathematics Handbook*, CRC Press, Boca Raton, Florida, second edition, 1990.

Annex A

Target models in Rayleigh mixture reverberation

The standard fluctuating and non-fluctuating target models may be represented as special cases of a Swerling Type III target which is formed as an additive component (U) to the complex matched filter output (Z),

$$Y = Z + U \tag{A1}$$

where U is complex Gaussian distributed with mean μ and variance λ_0 and under the Rayleigh mixture distributed reverberation assumption, Z is distributed as a mixture of zero-mean complex Gaussian random variables with proportions π_i and variances λ_i for $i = 1, \ldots, p$,

$$f_Z(z;\Theta) = \sum_{i=1}^{p} \pi_i \frac{1}{\pi\lambda_i} e^{-\frac{|z|^2}{\lambda_i}}. \tag{A2}$$

Here, as in the main part of this report, $\Theta = [\pi_1 \ \cdots \ \pi_p \ \lambda_1 \ \cdots \ \lambda_p]$. The non-fluctuating model is obtained by setting $\lambda_0 = 0$ and the fluctuating model by setting $\mu = 0$.

The distribution of Y may be found by first conditioning on and then integrating over U,

$$f_Y(y;\Theta,\mu,\lambda_0) = \sum_{i=1}^{p} \pi_i \frac{1}{\pi(\lambda_0+\lambda_i)} e^{-\frac{|y-\mu|^2}{\lambda_0+\lambda_i}} \tag{A3}$$

which is seen to be a mixture of complex Gaussian random variables with mean μ and variance $\lambda_0 + \lambda_i$. When the mixture distribution is interpreted as one of the p reverberation models occurring with its associated probability, this target-plus-reverberation distribution is acceptable on an intuitive level as the target introduces the same effect on each reverberation component when it occurs.

By transforming the real and imaginary parts of Y to magnitude and angle coordinates, followed by integration over the angle coordinate, the distribution of the matched filter magnitude output ($X = |Y|$) is found,

$$\begin{aligned} f(x;\Theta,\mu,\lambda_0) &= \sum_{i=1}^{p} \pi_i \frac{2x}{\lambda_0+\lambda_i} e^{-\frac{\left(x^2+|\mu|^2\right)}{\lambda_0+\lambda_i}} I_0\left(\frac{2x|\mu|}{\lambda_0+\lambda_i}\right) \\ &= \sum_{i=1}^{p} \pi_i \frac{2x}{\lambda_0+\lambda_i} e^{-\delta_i - \frac{x^2}{\lambda_0+\lambda_i}} I_0\left(2x\sqrt{\frac{\delta_i}{\lambda_0+\lambda_i}}\right) \end{aligned}$$

$$= \sum_{i=1}^{p} \pi_i \, f_1 \left(x; \lambda_0 + \lambda_i, \delta_i \right) \tag{A4}$$

where $\delta_i = \frac{|\mu|^2}{\lambda_0 + \lambda_i}$ is a signal-to-reverberation power ratio (SRR) for each reverberation component,

$$f_1 \left(x; \lambda, \delta \right) = \frac{2x}{\lambda} \mathrm{e}^{-\delta - \frac{x^2}{\lambda}} \, I_0 \left(2x \sqrt{\frac{\delta}{\lambda}} \right) \tag{A5}$$

is the Rician distribution with scale parameter λ and SRR parameter δ, and $I_0 \left(x \right)$ is the zero-order modified Bessel function. Thus, the magnitude matched filter output is a mixture of Rician random variables with scales $\lambda_0 + \lambda_i$ and SRRs δ_i. A non-fluctuating target ($\lambda_0 = 0$) results in a mixture of Rician random variables with scales λ_i and SRR parameters $\frac{|\mu|^2}{\lambda_i}$,

$$f_{\mathrm{nf}} \left(x; \Theta, \mu \right) = \sum_{i=1}^{p} \pi_i \, f_1 \left(x; \lambda_i, \frac{|\mu|^2}{\lambda_i} \right). \tag{A6}$$

A fluctuating target ($\mu = 0$) results in a mixture of Rayleigh random variables with power $\lambda_0 + \lambda_i$,

$$f_{\mathrm{fl}} \left(x; \Theta, \lambda_0 \right) = \sum_{i=1}^{p} \pi_i \, \frac{2x}{\lambda_0 + \lambda_i} \mathrm{e}^{-\frac{x^2}{\lambda_0 + \lambda_i}}. \tag{A7}$$

Annex B

Derivation of the EM parameter estimates for a Rayleigh mixture

The premise of the EM algorithm lies in the ability to describe the observed data as being part of a larger set of data with a simpler likelihood function for the unknown parameters. In the case of a mixture model, there is a very natural complete set of data. If a random variable is drawn from the distribution $f(x;\lambda_i)$ with probability π_i for $i = 1, \ldots, p$, then it has the mixture PDF described in eq. (12). Observing just the reverberation samples $\{x_1, x_2, \ldots, x_n\}$ the missing data are simply the indices that indicate which distribution x_j was drawn from; that is,

$$K_j = i \tag{B1}$$

if x_j comes from mixture component i for $j = 1, \ldots, n$. The PDF of the complete data is

$$f(\mathbf{x}, \mathbf{K}; \Theta) = \prod_{j=1}^{n} \pi_{K_j} f\left(x_j; \lambda_{K_j}\right) \tag{B2}$$

where $\mathbf{x} = [x_1 \ \cdots \ x_n]^T$ and $\mathbf{K} = [K_1 \ \cdots \ K_n]^T$. Note that K_j can take on integer values from 1 to p, the number of mixture components. Denote as the set of all possible values of $\mathbf{K}$

$$\Psi_K = \{1,\ 2,\ \ldots,\ p\}^n . \tag{B3}$$

The PDF of the missing data $\mathbf{K}$ conditioned on the observed data $\mathbf{x}$ is

$$\begin{aligned} f(\mathbf{K}\,|\mathbf{x};\Theta) &= \frac{f(\mathbf{x}, \mathbf{K}; \Theta)}{f(\mathbf{x};\Theta)} \\ &= \frac{\prod_{j=1}^{n} \pi_{K_j} f\left(x_j; \lambda_{K_j}\right)}{\prod_{j=1}^{n} \sum_{i=1}^{p} \pi_i\, f(x_j;\lambda_i)} \\ &= \prod_{j=1}^{n} W_{K_j,j} \end{aligned} \tag{B4}$$

where

$$f(\mathbf{r};\Theta) = \prod_{j=1}^{n} \sum_{i=1}^{p} \pi_i\, f(x_j;\lambda_i) \tag{B5}$$

is the joint PDF of the observed data and

$$W_{K_j,j} = \frac{\pi_{K_j} f\left(x_j; \lambda_{K_j}\right)}{\sum_{i=1}^{p} \pi_i \, f\left(x_j; \lambda_i\right)}. \tag{B6}$$

The expectation step of the EM-algorithm requires forming the expected value of the log-likelihood function of the complete data where the expectation is taken over the missing data conditioned on the observed data,

$$\begin{aligned} Q\left(\Theta, \Theta'\right) &= \mathrm{E}_{\Theta'}\left[\log f\left(\mathbf{x}, \mathbf{K}; \Theta\right)\right] \\ &= \sum_{\mathbf{K} \in \Psi_K} \log\left[f\left(\mathbf{x}, \mathbf{K}; \Theta\right)\right] f\left(\mathbf{K} \,|\mathbf{x}; \Theta'\right) \\ &= \sum_{\mathbf{K} \in \Psi_K} \left\{ \sum_{j=1}^{n} \left[\log \pi_{K_j} + \log 2x_j - \log \lambda_{K_j} - \frac{x_j^2}{\lambda_{K_j}} \right] \right\} \left[\prod_{j=1}^{n} W'_{K_j,j} \right] \\ &= \sum_{i=1}^{p} \sum_{j=1}^{n} W'_{i,j} \left[\log \pi_i + \log 2x_j - \log \lambda_i - \frac{x_j^2}{\lambda_i} \right] \end{aligned} \tag{B7}$$

where $W'_{i,j}$ is formed from the values in Θ' and the simplification

$$\sum_{K_j=1}^{p} W'_{K_j,j} = 1 \tag{B8}$$

has been used.

The maximization step of the EM-algorithm requires choosing Θ (i.e., the π_i and λ_i) to maximize $Q\left(\Theta, \Theta'\right)$ constraining $\sum_{i=1}^{p} \pi_i = 1$ and perhaps requiring each individual proportion $\pi_i \geq 0$. Using a Lagrange multiplier to enforce the first constraint, it is easily shown that maximizing $Q\left(\Theta, \Theta'\right)$ with respect to π_i requires choosing

$$\hat{\pi}_i = \frac{1}{n} \sum_{j=1}^{n} W'_{i,j}. \tag{B9}$$

This particular choice for the mixture proportions also satisfies the latter constraint mentioned above $\hat{\pi}_i \geq 0$. Maximizing $Q\left(\Theta, \Theta'\right)$ with respect to λ_i results in choosing

$$\hat{\lambda}_i = \frac{\sum_{j=1}^{n} x_j^2 W'_{i,j}}{\sum_{j=1}^{n} W'_{i,j}}. \tag{B10}$$

Annex C
Mean and variance of T_m

The mean and variance of the target pruning statistic T_m described in eq. (29) must be determined in order to use a Gaussian approximation to obtain thresholds according to the Type I error probability. Throughout this annex, the following summations [29] have been used liberally,

$$\sum_{k=1}^{n} k = \frac{n\,(n+1)}{2}, \tag{C1}$$

$$\sum_{k=1}^{n} k^2 = \frac{n\,(n+1)\,(2n+1)}{6}, \tag{C2}$$

$$\sum_{k=1}^{n} k^3 = \frac{n^2\,(n+1)^2}{4}, \tag{C3}$$

and

$$\sum_{k=1}^{n} k^4 = \frac{n\,(n+1)\,(2n+1)\,(3n^2+3n-1)}{30}. \tag{C4}$$

It is instructive to first consider the case of $T_2 = (K_1 - K_2)^2$ as the PMF may be obtained analytically and used to verify more general results. As K_1 and K_2 can take on any integer values from 1 to n as long as they are not equal, there are $n\,(n-1)$ equally likely combinations. Throughout these combinations, there are exactly $2\,(n-j)$ where $|K_1 - K_2| = j$ for $j = 1, \ldots, n-1$. Thus, the PMF of T_2 is

$$f_2\,[t] = \begin{cases} \frac{2(n-\sqrt{t})}{n(n-1)} & \text{if } \sqrt{t} = 1, \ldots, n-1 \\ 0 & \text{otherwise} \end{cases}. \tag{C5}$$

It is now straightforward to determine the mean T_2,

$$\begin{aligned} \mathrm{E}\,[T_2] &= \sum_{j=1}^{n-1} 2j^2 \frac{(n-j)}{n\,(n-1)} \\ &= \frac{n\,(n+1)}{6}. \end{aligned} \tag{C6}$$

The power of T_2 may be similarly obtained through direct summation over the PMF; however, obtaining it from the definition will help with the derivation of the general case,

$$\begin{aligned} \mathrm{E}\left[T_2^2\right] &= \mathrm{E}\left[(K_1 - K_2)^4\right] \\ &= \mathrm{E}\left[K_1^4\right] - 4\mathrm{E}\left[K_1^3 K_2\right] + 6\mathrm{E}\left[K_1^2 K_2^2\right] - 4\mathrm{E}\left[K_1 K_2^3\right] + \mathrm{E}\left[K_2^4\right]. \end{aligned} \quad \text{(C7)}$$

Due to the symmetry in the joint PMF of the indices to the order statistics, the exact index or indices in the above expectations are not relevant. For example,

$$\begin{aligned} c_1 &= \mathrm{E}\left[K_1^4\right] = \mathrm{E}\left[K_2^4\right] = \mathrm{E}\left[K_i^4\right] \\ &= \sum_{i=1}^{n} \frac{i^4}{n} \\ &= \frac{(n+1)(2n+1)(3n^2+3n-1)}{30} \end{aligned} \quad \text{(C8)}$$

and

$$\begin{aligned} c_2 &= \mathrm{E}\left[K_1^3 K_2\right] = \mathrm{E}\left[K_1 K_2^3\right] = \mathrm{E}\left[K_i K_j^3\right] \\ &= \frac{1}{n(n-1)}\left[\sum_{i=1}^{n}\left(\sum_{j=1}^{n} ij^3 - i^4\right)\right] \\ &= \frac{1}{n(n-1)}\left[\sum_{i=1}^{n} i \sum_{j=1}^{n} j^3 - \sum_{i=1}^{n} i^4\right] \\ &= \frac{(n+1)(15n^3+21n^2-4)}{120}. \end{aligned} \quad \text{(C9)}$$

In the latter case, note that using summations from 1 to n for each index requires removing the terms where $K_1 = K_2$. Similarly,

$$\begin{aligned} c_3 &= \mathrm{E}\left[K_1^2 K_2^2\right] \\ &= \frac{1}{n(n-1)}\left[\sum_{i=1}^{n}\left(\sum_{j=1}^{n} i^2 j^2 - i^4\right)\right] \\ &= \frac{1}{n(n-1)}\left[\left(\sum_{i=1}^{n} i^2\right)^2 - \sum_{i=1}^{n} i^4\right] \\ &= \frac{(n+1)(2n+1)}{180(n-1)}\left(10n^3 - 3n^2 - 13n + 6\right). \end{aligned} \quad \text{(C10)}$$

Substitution into eq. (C7) results in

$$\mathrm{E}\left[T_2^2\right] = 2c_1 - 8c_2 + 6c_3. \quad \text{(C11)}$$

The more general case is described by eq. (29) in non-recursive form and repeated here for convenience,

$$T_m = \sum_{i=2}^{m} \sum_{j=1}^{i-1} (K_i - K_j)^2 . \tag{C12}$$

The mean of T_m is then easily found from the mean of T_2,

$$\begin{aligned} \mathrm{E}[T_m] &= \sum_{i=2}^{m} \sum_{j=1}^{i-1} \mathrm{E}\left[(K_i - K_j)^2\right] \\ &= \left[\frac{m(m-1)}{2}\right] \mathrm{E}[T_2] \\ &= \left[\frac{m(m-1)}{2}\right] \left[\frac{n(n+1)}{6}\right] \\ &= l \left[\frac{n(n+1)}{6}\right], \end{aligned} \tag{C13}$$

where $l = \frac{m(m-1)}{2}$ is the number of terms in the double summation. The power of T_m may be described as

$$\mathrm{E}\left[T_m^2\right] = \sum_{i=2}^{m} \sum_{j=1}^{i-1} \sum_{k=2}^{m} \sum_{l=1}^{k-1} \mathrm{E}\left[(K_i - K_j)^2 (K_k - K_l)^2\right] \tag{C14}$$

$$\begin{aligned} &= l\, \mathrm{E}\left[(K_1 - K_2)^4\right] + l_0\, \mathrm{E}\left[(K_1 - K_2)^2 (K_3 - K_4)^2\right] \\ &\quad + \left[l(l-1) - l_0\right] \mathrm{E}\left[(K_1 - K_2)^2 (K_1 - K_3)^2\right], \end{aligned} \tag{C15}$$

where

$$l_0 = \begin{cases} 6\binom{m}{4} & m \geq 4 \\ 0 & m < 4 \end{cases} . \tag{C16}$$

The four summations of eq. (C14) result in l^2 terms, of which l are cases where the index pairs (i,j) and (k,l) are the same (i.e., $i = k$ and $j = l$ or $i = l$ and $j = k$), $l(l-1) - l_0$ are cases where the pairs share only one common index, and l_0 are cases where all four indices are different. The value of l_0 described in eq. (C16) is obtained by noting that for each set of four indices there are six combinations that occur in the summations of eq. (C14); for example, the combinations

$$(K_4 - K_3)^2 (K_2 - K_1)^2, \quad (K_4 - K_2)^2 (K_3 - K_1)^2, \quad (K_4 - K_1)^2 (K_3 - K_2)^2 \tag{C17}$$

occur as do their reverse multiplicative order. A similar argument may be used to show that the number of combinations with one common index is

$$l(l-1) - l_0 = 6\binom{m}{3} \tag{C18}$$

for $m \geq 3$.

From eqs. (C7) and (C11) the first expectation in eq. (C15) is seen to be

$$\mathrm{E}\left[(K_1 - K_2)^4\right] = 2c_1 - 8c_2 + 6c_3. \tag{C19}$$

The second expectation results in

$$\begin{aligned}
\mathrm{E}\left[(K_1 - K_2)^2 (K_3 - K_4)^2\right] &= \mathrm{E}\left[\begin{array}{r} 4K_1K_2K_3K_4 + K_1^2K_3^2 - 2K_1^2K_3K_4 \\ +K_1^2K_4^2 - 2K_2^2K_3K_4 \\ +K_2^2K_3^2 - 2K_3^2K_1K_2 \\ +K_2^2K_4^2 - 2K_4^2K_1K_2 \end{array}\right] \\
&= 4c_3 + 4c_4 - 8c_5,
\end{aligned} \tag{C20}$$

where

$$\begin{aligned}
c_4 &= \mathrm{E}\left[K_1K_2K_3K_4\right] \\
&= \frac{(n-4)!}{n!}\sum_{i=1}^{N} i\left\{\sum_{j=1}^{n} j\left[\sum_{k=1}^{n} k\left(\sum_{l=1}^{n} l - i - j - k\right)\right.\right. \\
&\qquad \left. -j\left(\sum_{l=1}^{n} l - i - 2j\right) - i\left(\sum_{l=1}^{n} l - j - 2i\right)\right] \\
&\qquad \left. -i\left[\sum_{k=1}^{n} k\left(\sum_{l=1}^{n} l - 2i - k\right) - 2i\left(\sum_{l=1}^{n} l - 3i\right)\right]\right\} \\
&= \frac{(n-4)!}{n!}\left\{\left[\sum_{i=1}^{n} i\right]^4 - 6\sum_{i=1}^{n} i^2\left[\sum_{j=1}^{n} j\right]^2 + 3\left[\sum_{i=1}^{n} i^2\right]^2 + 8\sum_{i=1}^{n} i\sum_{j=1}^{n} j^3 - 6\sum_{i=1}^{n} i^4\right\} \\
&= \frac{(n+1)\left[15n^2(n+1)^2(n-4) + 4(2n+1)(10n^2+9n-4)\right]}{240(n-1)(n-2)}
\end{aligned} \tag{C21}$$

and

$$\begin{aligned}
c_5 &= \mathrm{E}\left[K_1^2K_2K_3\right] \\
&= \frac{(n-3)!}{n!}\sum_{i=1}^{N} i^2\left\{\sum_{j=1}^{n} j\left[\sum_{k=1}^{n} k - j - i\right] - i\left[\sum_{k=1}^{n} k - 2i\right]\right\} \\
&= \frac{(n-3)!}{n!}\left\{\sum_{i=1}^{N} i^2\left[\sum_{j=1}^{n} j\right]^2 - \left[\sum_{i=1}^{n} i^2\right]^2 - 2\sum_{i=1}^{n} i^3\sum_{j=1}^{n} j + 2\sum_{i=1}^{n} i^4\right\} \\
&= \frac{(n+1)\left[15n^2(n+1)^2(2n-5) - 2(2n+1)(10n^3 - 21n^2 - 31n + 12)\right]}{360(n-1)(n-2)}.
\end{aligned} \tag{C22}$$

The third expectation results in

$$\begin{aligned} \mathrm{E}\left[(K_1-K_2)^2(K_1-K_3)^2\right] &= \mathrm{E}\left[\begin{array}{r} K_1^4-2K_1^3K_3+K_1^2K_2^2+4K_1^2K_2K_3 \\ -2K_1^3K_2+K_1^2K_3^2-2K_3^2K_1K_2 \\ +K_2^2K_3^2-2K_2^2K_1K_3 \end{array}\right] \\ &= c_1-4c_2+3c_3+0c_5 \\ &= c_1-4c_2+3c_3. \end{aligned} \tag{C23}$$

Substituting eqs. (C19), (C20), and (C23) into eq. (C15) results in

$$\begin{aligned} \mathrm{E}\left[T_m^2\right] &= l(2c_1-8c_2+6c_3)+l_0(4c_3+4c_4-8c_5) \\ &\quad +[l(l-1)-l_0](c_1-4c_2+3c_3). \end{aligned} \tag{C24}$$

The variance of T_m may then be easily obtained from

$$\mathrm{Var}[T_m]=\mathrm{E}\left[T_m^2\right]-\mathrm{E}[T_m]^2. \tag{C25}$$

Annex D

Invariance of false alarm performance in Weibull reverberation using ML parameter estimates

If the maximum likelihood parameter estimates for Weibull distributed reverberation are used in the statistical normalizer nonlinearity of eq. (10), the false alarm performance is invariant over the whole family of Weibull distributions. A proof of the invariance follows in this annex.

Either by differentiating the joint PDF of Weibull distributed auxiliary data (X_1, ..., X_n) with respect to α and β or from the iteration described in [6], the following relationships may be derived for the ML parameter estimates

$$\hat{\alpha} = \left[\frac{1}{n}\sum_{i=1}^{n} X_i^{\hat{\beta}}\right]^{-1} \tag{D1}$$

and

$$\frac{1}{\hat{\beta}} = -\frac{1}{n}\sum_{i=1}^{n}\log X_i + \frac{\sum_{i=1}^{n} X_i^{\hat{\beta}}\log X_i}{\sum_{i=1}^{n} X_i^{\hat{\beta}}}. \tag{D2}$$

Letting $Z_i = \alpha X_i^{\beta}$ these relationships may be described as

$$\hat{\alpha} = \alpha^{\frac{\hat{\beta}}{\beta}}\left[\frac{1}{n}\sum_{i=1}^{n} Z_i^{\frac{\hat{\beta}}{\beta}}\right]^{-1} \tag{D3}$$

and

$$\frac{\beta}{\hat{\beta}} = -\frac{1}{n}\sum_{i=1}^{n}\log Z_i + \frac{\sum_{i=1}^{n} Z_i^{\frac{\hat{\beta}}{\beta}}\log Z_i}{\sum_{i=1}^{n} Z_i^{\frac{\hat{\beta}}{\beta}}}. \tag{D4}$$

If the X_i are Weibull with parameters α and β, then the Z_i are exponentially distributed with unit mean; that is, the Z_i are distributionally free from α and β. Thus, according to eq. (D4), the ratio $\frac{\hat{\beta}}{\beta}$ is also distributionally free from α and β.

Substituting eq. (D3) into the nonlinearity of eq. (10) using the ML parameter estimates results in

$$g(X) = \sqrt{\hat{\alpha}X^{\hat{\beta}}}$$

$$= \left[\frac{Z^{\frac{\hat{\beta}}{\beta}}}{\frac{1}{n}\sum_{i=1}^{n} Z_i^{\frac{\hat{\beta}}{\beta}}} \right]^{\frac{1}{2}} \tag{D5}$$

where $Z = \alpha X^{\beta}$ is exponentially distributed if X is Weibull distributed with parameters α and β. Thus, $g(X)$ is distributionally free from α and β resulting in a constant false alarm probability irrespective of the actual values of α and β.

Substituting eq. (D3) into the instantaneous P_{fa} of eq. (40) similarly shows a lack of distributional dependence on α and β,

$$P_{fa}\left(\hat{\Theta}, h\right) = \exp\left\{ -\left(\frac{h^2}{n} \sum_{i=1}^{n} Z_i^{\frac{\hat{\beta}}{\beta}} \right)^{\frac{\beta}{\hat{\beta}}} \right\}. \tag{D6}$$

Document Data Sheet

Security Classification		Project No.
UNCLASSIFIED		041-3
Document Serial No.	**Date of Issue**	**Total Pages**
SR-303	August 1999	65 pp.

Author(s)

Abraham, D.A.

Title

Statistical normalization of non-Rayleigh reverberation

Abstract

Low-frequency active sonar systems operating in shallow water are primarily limited by reverberation. Reverberation is traditionally assumed to follow a Rayleigh probability distribution, from which the detector and other signal processing algorithms are developed. Experimental studies have shown that reverberation can be non-Rayleigh distributed with varying statistical character over range and bearing. In such a situation, detectors designed under a Rayleigh assumption will exhibit increased and varying false alarm performance. This report develops a technique for dealing with the unknown and varying reverberation statistics by using a non-Rayleigh reverberation model to perform a statistical normalization of the background reverberation. In this manner, range-bearing images will be produced that have a constant background reverberation distribution (i.e., Rayleigh). The technique is evaluated through simulation, with particular attention to the false alarm performance, which is seen to depend on the severity of the non-Rayleighness of the reverberation and the amount of data used to estimate the parameters of the reverberation model. Application to real data has shown that a large degree of the non-stationarity of the range-bearing image can be removed by statistical normalization.

Keywords

Non-Rayleigh – reverberation – constant false alarm rate - normalization

Issuing Organization

North Atlantic Treaty Organization
SACLANT Undersea Research Centre
Viale San Bartolomeo 400, 19138 La Spezia, Italy

[From N. America: SACLANTCEN (New York) APO AE 09613]

Tel: +39 0187 527 361
Fax:+39 0187 527 700

E-mail: library@saclantc.nato.int

The SACLANT Undersea Research Centre provides the Supreme Allied Commander Atlantic (SACLANT) with scientific and technical assistance under the terms of its NATO charter, which entered into force on 1 February 1963. Without prejudice to this main task - and under the policy direction of SACLANT - the Centre also renders scientific and technical assistance to the individual NATO nations.

This document is approved for public release.
Distribution is unlimited

SACLANT Undersea Research Centre
Viale San Bartolomeo 400
19138 San Bartolomeo (SP), Italy

tel: +39 0187 527 (1) or extension
fax: +39 0187 527 700

e-mail: library@saclantc.nato.int

NORTH ATLANTIC TREATY ORGANIZATION